Electronic Supplementary Material (ESI) for Chemical Science.
This journal is © The Royal Society of Chemistry 2015

Supporting information

Encapsulation of an organometallic cationic catalyst by direct exchange into an anionic MOF

Alexios Grigoropoulos,[a] George F. S. Whitehead,[a] Noémie Perret,[a] Alexandros P. Katsoulidis,[a] F. Mark Chadwick,[b] Robert P. Davies,[c] Anthony Haynes,[d] Lee Brammer,[d] Andrew S. Weller,[b*] Jianliang Xiao,[a] Matthew J. Rosseinsky[a*]

[a]Department of Chemistry, University of Liverpool, Liverpool L69 7ZD, U.K.
[b]Department of Chemistry, Chemistry Research Laboratories, University of Oxford, Mansfield Road, Oxford OX1 3TA, U.K.
[c]Department of Chemistry, Imperial College London, South Kensington, London SW7 2AZ, U.K.
[d]Department of Chemistry, University of Sheffield, Brook Hill, Sheffield S3 7HF, U.K.

Table of Contents

1. Materials, methods and instrumentation

Materials and Methods: All manipulations of air and moisture sensitive compounds were carried out using either standard Schlenk and cannula techniques or a MBraun glovebox. Anhydrous solvents were bought from Fisher, stored over pre-activated 4Å molecular sieves (120 °C under high vacuum for 20 h) and degassed before use (three freeze-pump-thaw cycles). All other solvents used (reagent-grade) were also bought from Fisher and uses as received. H_3BTB (benzene tribenzoic acid) was bought from Alpha-Aesar. $[CpFe(CO)_2(THF)][BF_4]$ ($[Fp\text{-}THF][BF_4]$) was bought from Santa-Kruz Biotechnologies and always stored below 0 °C inside the glovebox under argon. All other chemicals were bought from Sigma Aldrich. Isoprene was degassed three times prior to use, whereas methyl vinyl ketone (MVK) was degassed by bubbling N_2 for 30 min.

Characterization and Analysis:

Elemental analysis (C, H, N content) was performed using a Thermo EA1112 Flash CHNS-O Analyser.

Thermogravimetric analysis (TGA) was carried out using a Q2500 or Q500 TA instrument in the 25-700 ºC temperature range under a 10 ºC/min scan rate and an air flow of 50 mL/min.

Solution phase ^1H, ^{13}C, ^{31}P and ^{19}F NMR spectra were collected on a Bruker 400 MHz instrument after digestion in DCl/d^6-dmso (1/5 v/v). Shifts are reported relatively to residual solvent.

IR spectra were collected in the solid state on ATR mode using an FT-IR Perkin-Elmer Spectrum 100 spectrometer (4 cm^{-1} resolution, 16 scans collected after finely grinding the samples).

N_2 adsorption-desorption isotherms at 77 K were collected on a Micromeritics 3Flex instrument. Samples were gently shaken in acetone for 24 h and then activated under high vacuum at room temperature for 20 h before measuring. The specific surface area was calculated applying the BET model for the N_2 adsorption data over a range of pressures which was selected according to the consistency criteria of Rouquerol. Total pore volume was estimated from the N_2 adsorbed amount at $P/P_0 = 0.9$.

ICP-OES analysis was performed after digesting 10 mg of the respective sample in diluted HNO_3 (1/10 v/v).

GC analysis was performed using an Agilent Technologies 7890A gas chromatograph equipped with a programmed split/splitless injector and FID, employing a DB-WAXetr 60 m × 0.25 mm *i.d.*, 0.25 µm film thickness capillary column (Agilent J&W). Products composition was determined after calibration with the commercially available compound (figure S40). All samples were filtered via a 0.2 µm syringe filter (Acrodisc® GHP) before injection.

Scanning Electron Microscopy (SEM) imaging was performed with a Hitachi S-4800 Field Emission SEM. A small amount of sample powder was spread on a carbon tape attached to an aluminium stab and coated with a few nanometers thick layer of gold. SEM-EDX measurements were performed on the same instrument with an Oxford instruments EDX detector.

X-ray single-crystal data collection and analysis: Single-crystal X-ray diffraction data for $[(Cp_2Co)_x(TEA)_{3-x}][In_3(BTC)_4]$ were collected on a Rigaku MicroMax™-007 HF with a molybdenum rotating anode microfocus source and a Saturn 724+ detector. Data for structure $[Cp_2Co]_3[In_3(BTC)_4]$ were collected on beamline I19 at Diamond Light Source. Structures were solved and refined using SHELX-2013.[1] In both cases the crystals contain solvent accessible voids, although the location of discrete solvent molecules could not be determined. The hydrogen atoms were placed in calculated positions using built-in SHELX riding models and assigned isotropic thermal parameters 1.2 times those of their parent atoms. In the case of $[Cp_2Co]_3[In_3(BTC)_4]$, the interatomic distances of the atoms within the cobaltocenium were restrained to the average values found for $[Cp_2Co]^+$ cations in the CSD[2] using SHELX DFIX instructions. Enhanced rigid bond restraints were also applied to these atoms using SHELX RIGU instructions. All $[Cp_2Co]^+$ atoms were modelled using a PART -1 instruction to supress the generation of special position constraints. Full crystallographic details for all crystal structures are included in Table S5. CCDC 1417097-1417098 contain the supplementary crystallographic data for this paper. These data can be obtained free of charge from the Cambridge Crystallographic Data Centre via www.ccdc.cam.ac.uk/data_request/cif.

X-ray powder diffraction: XRPD patterns were collected in transmission geometry at 298 K on a Bruker D8 advance diffractometer with Cu K_α radiation ($\lambda = 1.54060$ Å). Samples were ground and transferred to a 0.5 mm internal diameter borosilicate capillary. Typically, profiles were collected over a 1 h period in the $5^o < 2\theta < 40^o$ range with a step size of 0.01°. Le Bail fitting[3] was performed using the PANanalytical X´Pert HyScore Plus program (version 2.2.1).

2. Synthesis

$[Me_2NH_2]_3[In_3(BTB)_4].12(DMF).16(H_2O)$ (ZJU-28) synthesis: The reported procedure[4,5] was modified and the stoichiometrically required ratio was used (In/H_3BTB = ¾) that in our hands leads to a single crystalline phase. If a higher molar ratio was used, then an unidentified insoluble amorphous phase was also formed in addition to ZJU-28. A mixture of solvents was prepared, as reported.[4,5] In a 100 mL round bottom flask 36 mL of DMF, 24 mL of dioxane, 4 mL of H_2O and 0.25 mL of HNO_3 were mixed under stirring. Subsequently stock solutions were prepared:

$InCl_3.4H_2O$: 1082 mg (3.69 mmol) were dissolved in 50 mL of the above solvent mixture ([In] = 0.074 M).

H_3BTB: 1100 mg (2.51 mmol) were dissolved in 50 mL of the above solvent mixture ([H_3BTB] = 0.050 M).

In a 40 mL vial with a teflon-lined screw cap, the solutions of $InCl_3.4H_2O$ (2.55 mL, 0.19 mmol) and H_3BTB (5.00 mL, 0.25 mmol) were added and then diluted with the solvent mixture (2.45 mL) to a total volume of 10 mL ([H_3BTB] = 0.025 M in the final reaction mixture). The vial was placed inside an oven, heated at 130 °C (1.0 °C/min ramping rate), maintained at 130 °C for 24 h and subsequently slowly cooled down to room temperature (0.2 °C/min cooling rate). White needle-shaped crystals precipitated upon cooling. They were collected by filtration, washed thoroughly with DMF (3 x 10 mL) and dried under vacuum until the particles could move freely (153 mg, 72%). Calculated for $C_{114}H_{84}In_3N_3O_{24}.12C_3H_7NO.16H_2O$ (FW = 3389.8): C, 53.15; H, 5.95; N, 6.20 Found: C, 52.81; H, 5.42; N, 6.67

$[(Me_2NH_2)(In_3(\mu\text{-}O)(H_2O)_3(BTC)_2][In_3(BTC)_4].8(DMF).22(H_2O)$ (CPM-5) synthesis: The reported procedure was followed.[6] Since $In(NO_3)_3.xH_2O$ is hygroscopic, indium concentration of a freshly prepared stock solution in DMF was determined by ICP-OES in order to properly adjust the stoichiometry between metal and linker to 3/4. Stock solutions were initially prepared:

$In(NO_3)_3.xH_2O$: 2007 mg was dissolved in 25 mL of DMF ([In] = 0.22 M from ICP).

H_3BTC: 1840 mg (8.76 mmol) were dissolved in 25 mL of DMF ([H_3BTC] = 0.35 M).

In a 40 mL vial with a teflon-lined screw cap, solutions of $In(NO_3)_3.xH_2O$ (2.35 mL, 0.52 mmol) and H_3BTC (2.00 mL, 0.70 mmol) were added and then diluted with DMF (1.65 mL) to a total volume of 6.0 mL ([H_3BTC] = 0.12 M in the final reaction mixture). The vial was placed inside an oven, heated at 120 °C (1.0 °C/min ramping rate), maintained at 120 °C for 5 days and subsequently slowly cooled down to room temperature (0.2 °C/min cooling rate). White cube-shaped crystals precipitated upon cooling. They were collected by filtration, washed thoroughly with DMF (3 x 10 mL) and EtOH (3 x 10 mL) and dried under vacuum until the particles could move freely (214 mg, 63%). Calculated for $C_{74}H_{44}In_9NO_{56}$.8C_3H_7NO.23H_2O (FW = 3875.6): C, 30.37 H, 3.80; N, 3.25 Found: C, 30.30; H, 3.66; N, 3.59

[Et_4N]$_3$[In_3(BTC)$_4$].2(DMF).5(H_2O) synthesis: The reported procedure was slightly modified and DMF was used as the solvent instead of DEF.[7] Since In(NO_3)$_3$.xH_2O is hygroscopic, indium concentration of a freshly prepared stock solution in DMF was determined by ICP-OES in order to properly adjust the stoichiometry between metal and linker to 3/4 and avoid formation of CPM-5 as a by-product. Stock solutions were initially prepared:

In(NO_3)$_3$.xH_2O: 2015 mg were dissolved in 25 mL of DMF ([In] = 0.23 M from ICP).
H_3BTC: 1044 mg (4.97 mmol) were dissolved in 25 mL of DMF ([H_3BTC] = 0.20 M).
Et_4NBr: 500 mg (2.38 mmol) were dissolved in 25 mL of DMF ([Et_4NBr] = 0.095 M).

In a 40 mL vial with a teflon-lined screw cap, solutions of In(NO_3)$_3$.xH_2O (1.31 mL, 0.30 mmol), H_3BTC (2.00 mL, 0.40 mmol) and Et_4NBr (3.13 mL, 0.30 mmol) were added and then diluted with DMF (3.56 mL) to a total volume of 10.0 mL ([H_3BTC] = 0.040 M in the final reaction mixture). The vial was placed inside an oven, heated at 120 °C (1.0 °C/min ramping rate), maintained at 120 °C for 4 days and subsequently slowly cooled down to room temperature (0.2 °C/min cooling rate). White cube-shaped crystals precipitated upon cooling. They were collected by filtration, washed thoroughly with DMF (3 x 10 mL), H_2O (1 x 10 mL) and MeOH (2 x 10 mL) and dried under vacuum until the particles could move freely (158 mg, 87%). Calculated for $C_{60}H_{72}In_3N_3O_{24}$.2($C_3H_7NO$).5($H_2O$) (FW = 1800.0): C, 44.04 H, 5.39; N, 3.89 Found: C, 43.90; H, 5.04; N, 4.25

[*n*Pr_4N]$_3$[In_3(BTC)$_4$]) synthesis: The reported procedure was followed.[7] Since In(NO_3)$_3$.xH_2O is hygroscopic, indium concentration of a freshly prepared stock solution in DMF was determined by ICP-OES in order to properly adjust the stoichiometry between metal and linker to 3/4. Stock solutions were initially prepared:

In(NO_3)$_3$.xH_2O: 5266 mg were dissolved in 50 mL of DMF ([In] = 0.29 M from ICP).
H_3BTC: 3694 mg (17.58 mmol) were dissolved in 50 mL of DMF ([H_3BTC] = 0.35 M).

Pr_4NBr: 2360 mg (8.86 mmol) were dissolved in 25 mL of DMF ([Bu_4NBr] = 0.35 M).

In a 40 mL vial with a teflon-lined screw cap, solutions of $In(NO_3)_3.xH_2O$ (1.51 mL, 0.44 mmol), H_3BTC (2.00 mL, 0.70 mmol) and Pr_4NBr (1.49 mL, 0.52 mmol) were added and then diluted with DMF (9.01 mL) to a total volume of 14.0 mL ([H_3BTC] = 0.050 M in the final reaction mixture). The vial was placed inside an oven, heated at 120 °C (1.0 °C/min ramping rate), maintained at 120 °C for 4 days and subsequently slowly cooled down to room temperature (0.2 °C/min cooling rate). White cube-shaped crystals precipitated upon cooling. They were collected by filtration, washed thoroughly with DMF (2 x 10 mL), H_2O (1 x 10 mL) and MeOH (2 x 10 mL) and dried under vacuum until the particles could move freely (234 mg, 92% based on In). Calculated for $C_{72}H_{96}In_3N_3O_{24}$ (FW = 1732.0): C, 49.93 H, 5.59; N, 2.43 Found: C, 49.36; H, 5.48; N, 2.41

[*n*Bu_4N]$_3$[$In_3(BTC)_4$] synthesis: The reported procedure was slightly modified and Bu_4NBr was used instead of Bu_4NF.[7] Since $In(NO_3)_3.xH_2O$ is hygroscopic, indium concentration of a freshly prepared stock solution in DMF was determined by ICP-OES in order to properly adjust the stoichiometry between metal and linker to 3/4. Stock solutions were initially prepared:

$In(NO_3)_3.xH_2O$: 5266 mg are dissolved in 50 mL of DMF ([In] = 0.29 M from ICP).

H_3BTC: 3694 mg (17.58 mmol) were dissolved in 50 mL of DMF ([H_3BTC] = 0.35 M).

Bu_4NBr: 2900 mg (9.00 mmol) were dissolved in 25 mL of DMF ([Bu_4NBr] = 0.36 M).

In a 40 mL vial with a teflon-lined screw cap, solutions of $In(NO_3)_3.xH_2O$ (1.51 mL, 0.44 mmol), H_3BTC (2.00 mL, 0.70 mmol) and Bu_4NBr (1.47 mL, 0.53 mmol) were added and then diluted with DMF (10.03 mL) to a total volume of 15.0 mL ([H_3BTC] = 0.047 M in the final reaction mixture). The vial was placed inside an oven, heated at 120 °C (1.0 °C/min ramping rate), maintained at 120 °C for 4 days and subsequently slowly cooled down to room temperature (0.2 °C/min cooling rate). White cube-shaped crystals precipitated upon cooling. They were collected by filtration, washed thoroughly with DMF (2 x 10 mL)), H_2O (1 x 10 mL) and MeOH (2 x 10 mL) and dried under vacuum until the particles could move freely (197 mg, 71% based on In). Calculated for $C_{84}H_{120}In_3N_3O_{24}$ (FW = 1900.3): C, 53.09 H, 6.38; N, 2.21 Found: C, 52.71; H, 6.27; N, 2.16

Stability tests: 80 mg of the respective MOF were added in a Schlenk tube. Subsequently, 10 mL of dry solvent were added and the tube was shaken gently for 1 day at room temperature. The supernatant was decanted, filtered through a syringe 0.2 μm filter (Acrodisc® GHP) and the filtrate was analyzed for indium leaching with ICP-OES. For all three MOFs, indium is not leaching in the supernatant ([In] < 0.1 ppm corresponding to < 0.05% leaching). The MOF was dried under vacuum until the particles could move freely. The PXRD pattern of the materials was collected. ZJU-28 does not retain its crystallinity in acetone or CH_2Cl_2 whereas all other MOFs tested remain crystalline (figures S1-S13).

Cobaltocenium cation exchange: Reaction was carried out under anaerobic conditions using dry solvents only for ZJU-28, but such precautions were not necessary for CPM-5 and $[R_4N]_3[In_3(BTC)_4]$) as both MOFs are stable in reagent-grade solvents. In a typical experiment, 100 mg of each MOF (ZJU-28, CPM-5 or $[R_4N]_3[In_3(BTC)_4]$) were added in a vial and subsequently a specific volume of a 0.02 M solution of $[Cp_2Co][PF_6]$ (66 mg, 0.198 mmol in 10 mL of acetone) was added in order to set un equimolar cation/$[Cp_2Co]^+$ ratio. The vial was gently shaken for a specific period of time (24, 48 and 72 h) during which the colour of the MOF progressively changed from white to yellow. The material was collected by filtration, washed thoroughly with acetone until the filtrate was colourless (3 x 10 mL) and dried under vacuum. Cobaltocenium exchange percentage was measured by ICP-OES after digestion in diluted HNO_3 (1/10 v/v), according to the following formula (Table S1):

$$\%\,exchange = \frac{\frac{[ppm\ Co]}{AW\ Co}}{\frac{[ppm\ In]}{AW\ In}} * \frac{number\ of\ In\ atoms}{total\ number\ of\ cations} * 100$$

Cobaltocenium exchange was also measured by ^1H NMR after digestion in DCl/dmso-d^6 (1/5 v/v), since $[Cp_2Co]^+$ survives digestion conditions (figure S14-S15, Table S2).

$[Cp_2Co]_3[In_3(BTC)_4]\cdot 3(DMF)\cdot 6(H_2O)$: Reaction was carried out in air using reagent-grade solvents. Stock solutions were initially prepared:

$InCl_3.4H_2O$: 948 mg (3.23 mmol) were dissolved in 25 mL of DMF ([In] = 0.129 M).
H_3BTC: 1064 mg (5.06 mmol) were dissolved in 25 mL of DMF ($[H_3BTC]$ = 0.20 M).
$[Cp_2Co][PF_6]$: 669 mg (2.00 mmol) were dissolved in 25 mL of DMF ($[Cp_2Co]$ = 0.080 M).
In a 40 mL vial with a teflon-lined screw cap, $InCl_3.4H_2O$ (2.35 mL, 0.303 mmol), H_3BTC (2.00 mL, 0.400 mmol) and $[Cp_2Co][PF_6]$ (3.80 mL, 0.304 mmol) were added and then diluted with DMF (1.86 mL) to a total volume of 10 mL ($[H_3BTC]$ = 0.040 M in the final reaction mixture). The vial was placed inside an oven, heated at 120 °C (1.0 °C/min ramping rate), maintained at 120 °C for 24 h days and subsequently slowly cooled down to room temperature (0.2 °C/min cooling rate). Yellow crystals precipitated upon cooling that were collected by filtration, washed thoroughly with DMF (3 x 10 mL) and MeOH (2 x 10 mL)

until the filtrate was colourless and dried under vacuum until the particles could move freely (131 mg were isolated, yield = 60%). Calculated for $C_{60}H_{72}In_3N_3O_{24}\cdot 3(C_3H_7NO)\cdot 6(H_2O)$ (FW = 2067.7): C, 43.57 H, 3.66; N, 2.03 Found: C, 43.56; H, 3.20; N, 1.95; In/Co = 0.98 (from ICP-OES)

$[CpFe(CO)_2L]^+$ cation exchange: Reaction was carried out under an inert atmosphere using standard Schlenk line techniques or an Ar atmosphere dry box. In a typical experiment, $[Et_4N]_3[In_3(BTC)_4].2(DMF).5(H_2O)$ (100 mg, 0.056 mmol) were immersed in 5 mL of dry acetone inside a Schlenk tube at room temperature and gentle shaking was applied for a total of 48 h during which the solvent was replenished once after 24 h. The solvent was decanted and the crystals were dried under high vacuum. A 0.02 M solution of $[Fp\text{-}THF][BF_4]$ (64 mg, 0.190 mmol) in 9 mL of dry and degassed acetone was prepared inside a Schlenk flask at 5 °C. The solution was transferred via a filter cannula inside the Schlenk tube containing the parent MOF, the tube was sealed under N_2 and kept in the refrigerator at 5 °C for 48 h. The supernatant was filtered off, the red-coloured crystals were washed twice with dry acetone and then soaked in dry acetone for two more days at 5 °C. Subsequently, the supernatant was filtered off and the material was dried under high vacuum until the particles could move freely. The isolated material was stored in a vial at -10 °C inside the glovebox where it is stable for at least 2 months. Cation exchange was determined by ICP-OES after digestion in diluted HNO_3 (1/10 v/v) according to the formula:

$$\%\,exchange = \frac{\frac{[ppm\,Fe]}{AW\,Fe}}{\frac{[ppm\,In]}{AW\,In}} *\ 100$$

Characterization of the catalyst was also carried out with the aid of IR spectroscopy, NMR spectroscopy in solution after digestion, TGA and PXRD. All spectroscopic evidence concur that $[Fp\text{-}L]^+$ remains intact during cation exchange, replacing 20% of the TEA cations and forming $[(Fp\text{-}L)_{0.6}(TEA)_{2.4}][In_3(BTC)_4]$ where the labile ligand (L) is most likely acetone.

CO experiments: Inside the glovebox, $[(Fp\text{-}L)_{0.6}(TEA)_{2.4}][In_3(BTC)_4]$ (25 mg) was added in a Schlenk flask capped with a rubber septum. The material was treated with a stream of CO gas for 15 min, during which the colour of the MOF changed from deep-red to orange yellow, indicating formation of $[Fp\text{-}CO]^+$. Subsequently, the Schlenk flask was mounted on the Schlenk line, pumped down and refilled with N_2 two times to remove excess of CO and the IR spectrum was collected, revealing three peaks in the *v*(CO) region due to partial formation of the tricarbonyl adduct (figure S31).

General procedure for heterogeneous Diels-Alder reactions: The catalytic reaction of MVK and isoprene is described. Reaction was carried out under an inert atmosphere using standard Schlenk line techniques or an Ar dry box. Freshly prepared solutions were used and kept at 5 °C:

MVK: 200 mL (2.465 mmol) were dissolved in 5 mL of dry and degassed CH_2Cl_2 ([MVK] = 0.493 M)

Isoprene: 500 mL (4.999 mmol) were dissolved in 10 mL of dry and degassed CH_2Cl_2 ([Iso] = 0.500 M)

Inside the glovebox, $[(Fp\text{-}L)_{0.6}(TEA)_{2.4}][In_3(BTC)_4]$ (38 mg, %Fe =1.9 from ICP, 0.013 mmol Fe) was added in a Schlenk tube. The Schlenk tube was mounted on the Schlenk line and cooled down to 5°C. MVK (0.25 mL = 0.123 mmol) and Iso (1.0 mL = 0.500 mmol) were added via a syringe and the tube was placed on a shaker. Gentle shaking was applied for the required time period. Subsequently, the supernatant was removed via a filter-cannula, filtered via a syringe filter (0.2 μm, Acrodisc® GHP) and analyzed by GC. Products yield was determined after calibration using the commercially available major product of the reaction (1-methyl-4-acetyl-cyclohexene, figure S40). Products composition was determined using an Agilent Technologies 7890A gas chromatograph equipped with a programmed split/splitless injector and FID, employing a DB-WAXetr 60 m × 0.25 mm *i.d.*, 0.25 μm film thickness capillary column (Agilent J&W). Repeated reactions delivered a product composition that was reproducible to within ± 2% (t_r = 4.67, Iso; t_r = 5.23, acetone; t_r = 6.08, MVK; t_r = 12.83, 1-methyl-5-acetyl-cyclohexene (minor DA product); t_r = 12.91, 1-methyl-4-acetyl-cyclohexene (major DA product). Major product was also characterized by ^1H and ^{13}C NMR spectroscopy after removing all the volatile compounds under vacuum and dissolving the organic residue in $CDCl_3$ (figure S41).

Recycling experiments: After the end of the first cycle (96 h), the supernatant was filtered off using a filter cannula and analyzed by GC (45% yield). The isolated $[(Fp\text{-}L)_{0.6}(TEA)_{2.4}][In_3(BTC)_4]$ catalyst was washed with dry CH_2Cl_2 (3 x 5 mL) and soaked in 5 mL of CH_2Cl_2 overnight at 5 °C. The next day, the supernatant was filtered off via a filter-cannula, the catalyst was dried under vacuum until the particles could move freely and a fresh batch of reactants was added under anaerobic conditions, as described in the general procedure for the heterogeneous DA reaction. The above process was repeated after the end of the 2nd cycle (42% yield). Yield for the 3rd cycle was 27%.

Leaching test: A heterogeneous DA reaction between Iso and MVK was set up as described above. After 24 h, the supernatant was filtered off via a filter-cannula and an aliquot of the filtrate (100 μL) was collected inside a glove-bag, filtered using a syringe filter (0.2 μm, Acrodisc® GHP) and analyzed by GC (12% yield). The filtrate was left to react for further 48 h and again an aliquot (100 μL) was collected inside a glove-bag, filtered using a syringe filter and analyzed by GC (14% yield). Yield was measured again after further 48 h by GC (14% yield).

General procedure for homogeneous Diels-Alder reactions: The catalytic reaction of MVK and isoprene is described. Freshly prepared solutions were used and kept at 5 °C:
MVK: 350 mL (4.314 mmol) in 8 mL of dry and degassed CH_2Cl_2 ([MVK] = 0.539 M)
Isoprene: 500 mL (4.999 mmol) in 10 mL of dry and degassed CH_2Cl_2 ([Iso] = 0.500 M)
Inside the glovebox, [Fp-THF][BF_4] (19 mg, 0.057 mmol Fe) was added in a Schlenk flask. The Schlenk flask was mounted on the Schlenk line and placed inside an ice-bath. MVK (1.00 mL, 0.539 mmol) and Iso (4.30 mL = 2.149 mmol) were added via a syringe and gentle stirring was applied for the required time period. Subsequently, the reaction mixture was passed through a silica gel pad (40 – 63 μm particle size), the pad was washed with reagent-grade CH_2Cl_2 (2 x 20 mL) and the filtrate was evaporated to approximately 1 mL total volume. The concentrated solution was diluted to 10 mL with CH_2Cl_2, passed through a syringe filter (0.2 μm, Acrodisc® GHP) and analyzed by GC. Yield was determined as described above. Major product was also characterized by ^1H and ^{13}C NMR spectroscopy after removing all the volatile compounds under vacuum and dissolving the organic residue in $CDCl_3$.

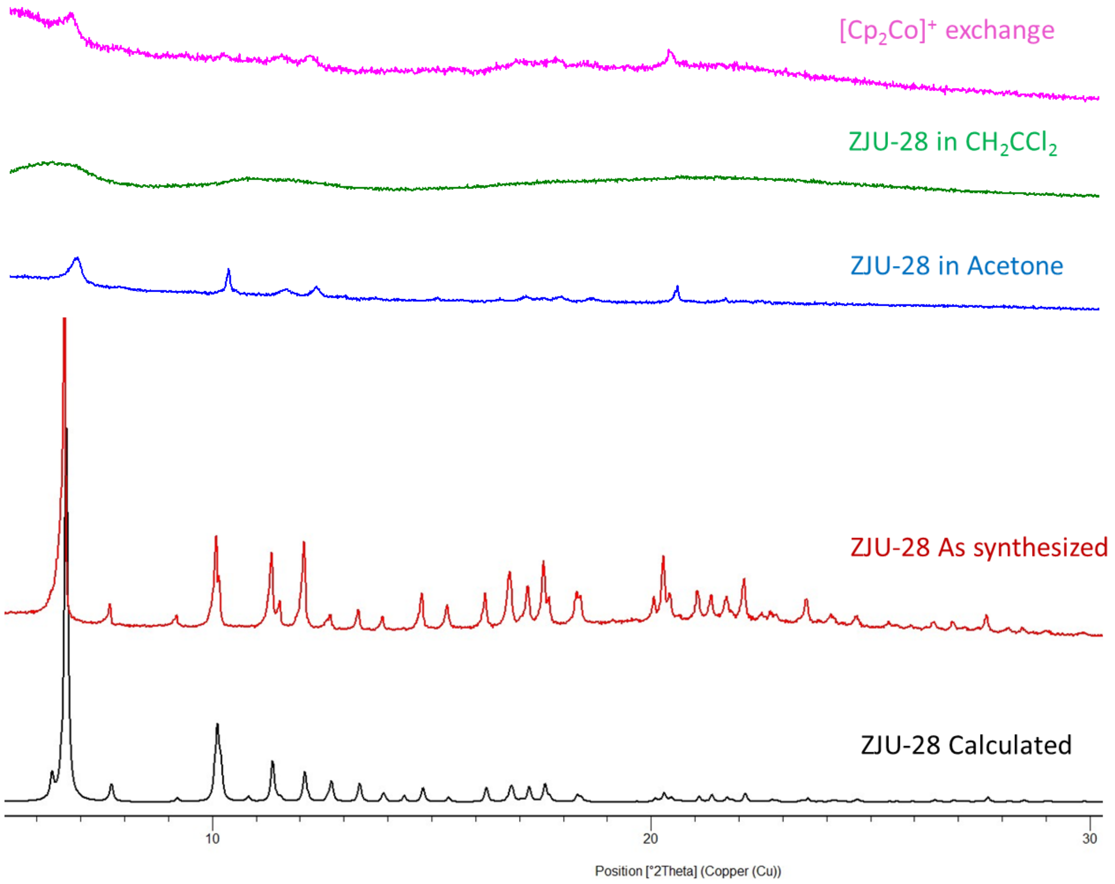

Figure S1. PXRD patterns of ZJU-28: calculated from the single crystal structure (black), as synthesized (red), after soaking in dry acetone (blue), dry CH_2Cl_2 (green) and after $[Cp_2Co]^+$ cation in dry acetone under anaerobic conditions (magenta). Crystallinity is not retained even when dry solvents are used.

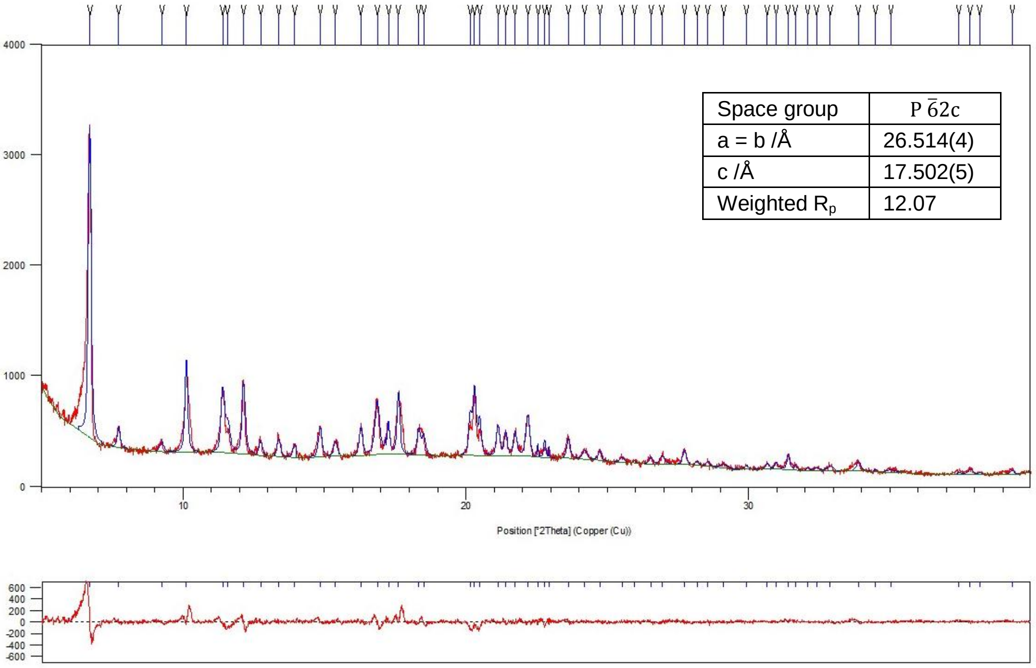

Space group	$P\bar{6}2c$
a = b /Å	26.514(4)
c /Å	17.502(5)
Weighted R_p	12.07

Figure S2. Le Bail fitting of PXRD pattern for as synthesized ZJU-28. Experimental pattern (red), calculated pattern (blue), difference pattern expt-calc (bottom). Unit cell dimensions determined from the fit and agreement indices are listed in the inset.

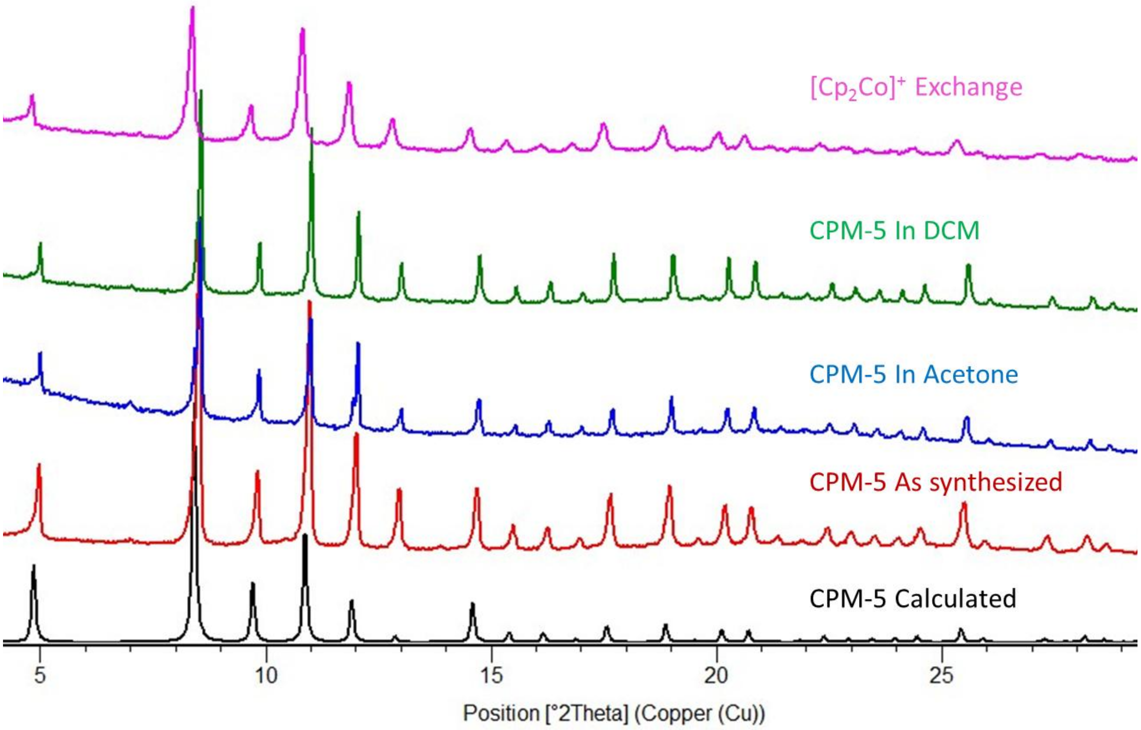

Figure S3. PXRD patterns of CPM-5: calculated from the single crystal structure (black), as synthesized (red), after soaking in acetone (blue), CH_2Cl_2 (green) and after $[Cp_2Co]^+$ cation exchange in acetone (magenta). CPM-5 remains crystalline under these conditions.

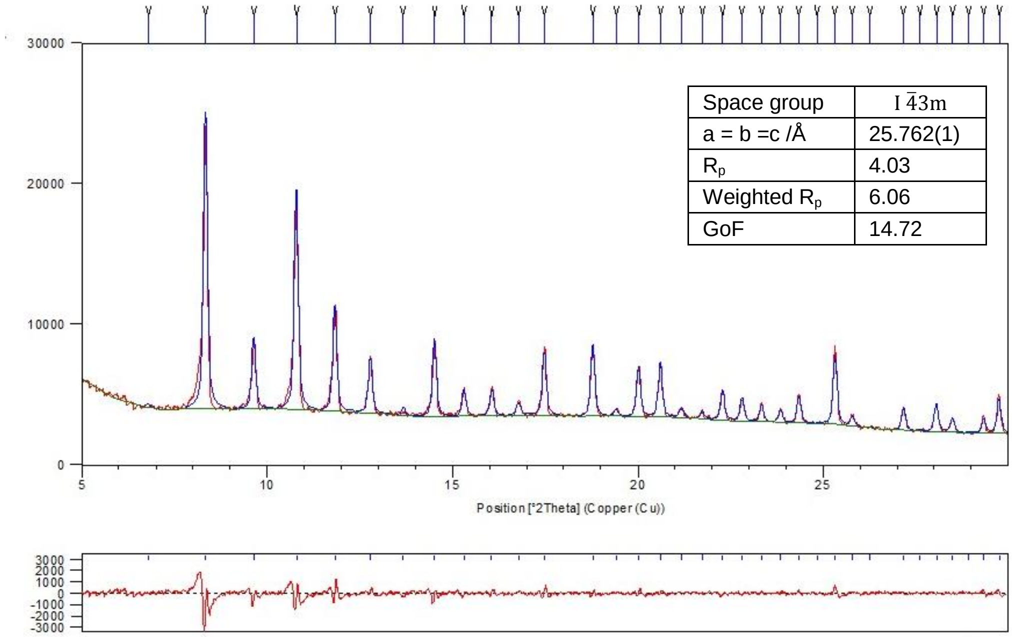

Space group	$I\bar{4}3m$
a = b =c /Å	25.762(1)
R_p	4.03
Weighted R_p	6.06
GoF	14.72

Figure S4. Le Bail fitting of PXRD pattern for as synthesized CPM-5. Experimental pattern (red), calculated pattern (blue), difference pattern expt-calc (bottom). Unit cell dimensions determined from the fit and agreement indices are listed in the inset.

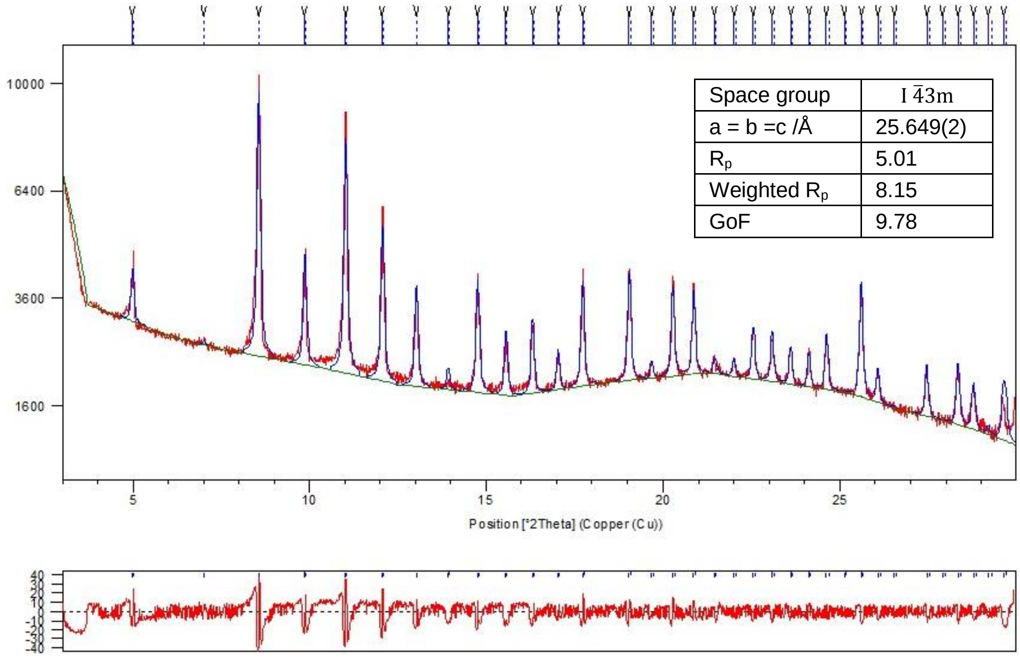

Space group	$I\bar{4}3m$
a = b =c /Å	25.649(2)
R_p	5.01
Weighted R_p	8.15
GoF	9.78

Figure S5. Le Bail fitting of PXRD pattern for CPM-5 after soaking in CH_2Cl_2. Experimental pattern (red), calculated pattern (blue), difference pattern expt-calc (bottom). Unit cell dimensions determined from the fit and agreement indices are listed in the inset.

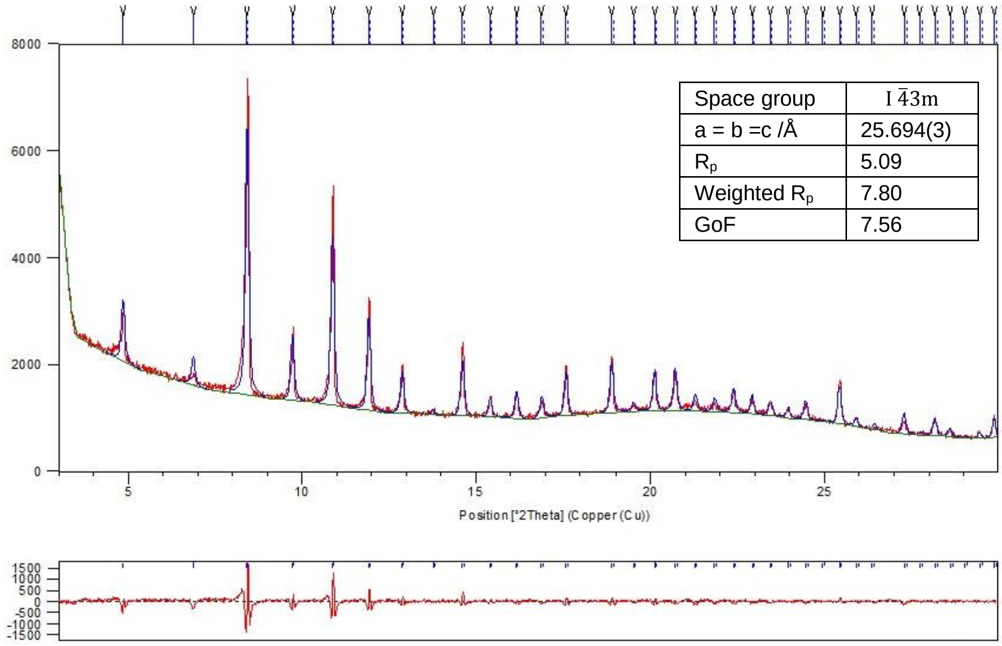

Space group	$I\bar{4}3m$
a = b =c /Å	25.694(3)
R_p	5.09
Weighted R_p	7.80
GoF	7.56

Figure S6. Le Bail fitting of PXRD pattern for CPM-5 after soaking in acetone. Experimental pattern (red), calculated pattern (blue), difference pattern expt-calc (bottom). Unit cell dimensions determined from the fit and agreement indices are listed in the inset.

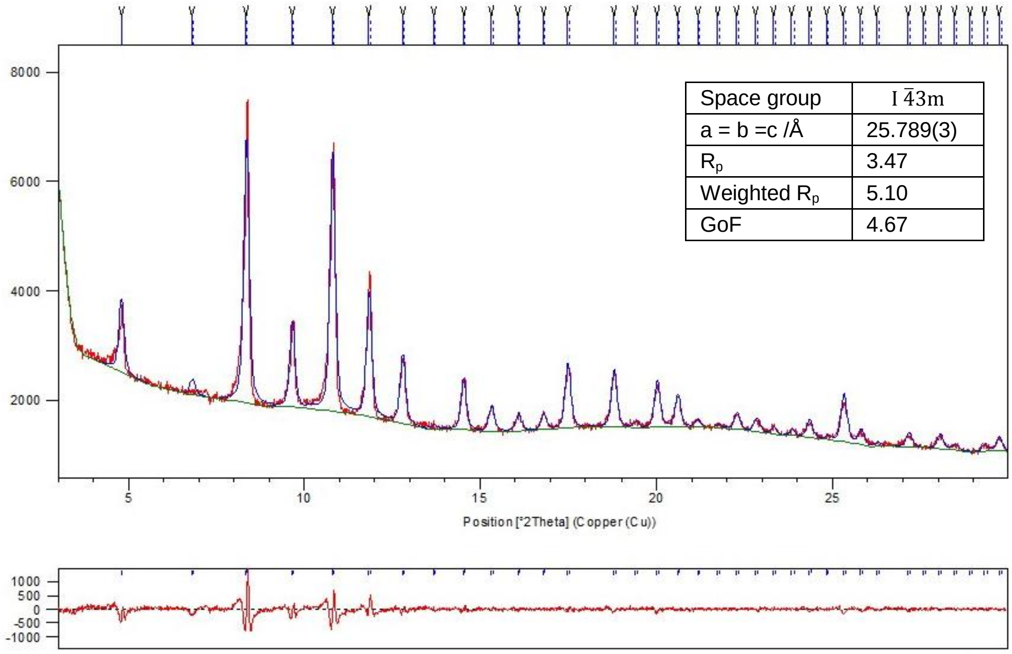

Space group	$I\bar{4}3m$
a = b =c /Å	25.789(3)
R_p	3.47
Weighted R_p	5.10
GoF	4.67

Figure S7. Le Bail fitting of PXRD pattern for CPM-5 after $[Cp_2Co]^+$ cation exchange in acetone. Experimental pattern (red), calculated pattern (blue), difference pattern expt-calc (bottom). Unit cell dimensions determined from the fit and agreement indices are listed in the inset.

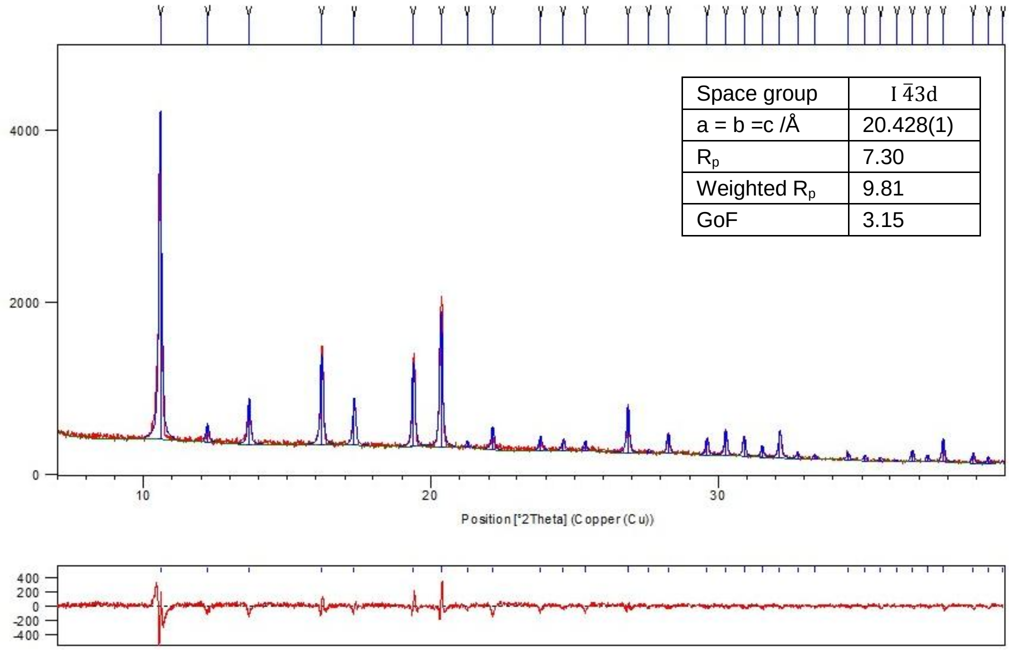

Space group	$I\bar{4}3d$
a = b =c /Å	20.428(1)
R_p	7.30
Weighted R_p	9.81
GoF	3.15

Figure S8. Le Bail fitting of PXRD pattern for as synthesized $[TEA]_3[In_3(BTC)_4]$. Experimental pattern (red), calculated pattern (blue), difference pattern expt-calc (bottom). Unit cell dimensions determined from the fit and agreement indices are listed in the inset.

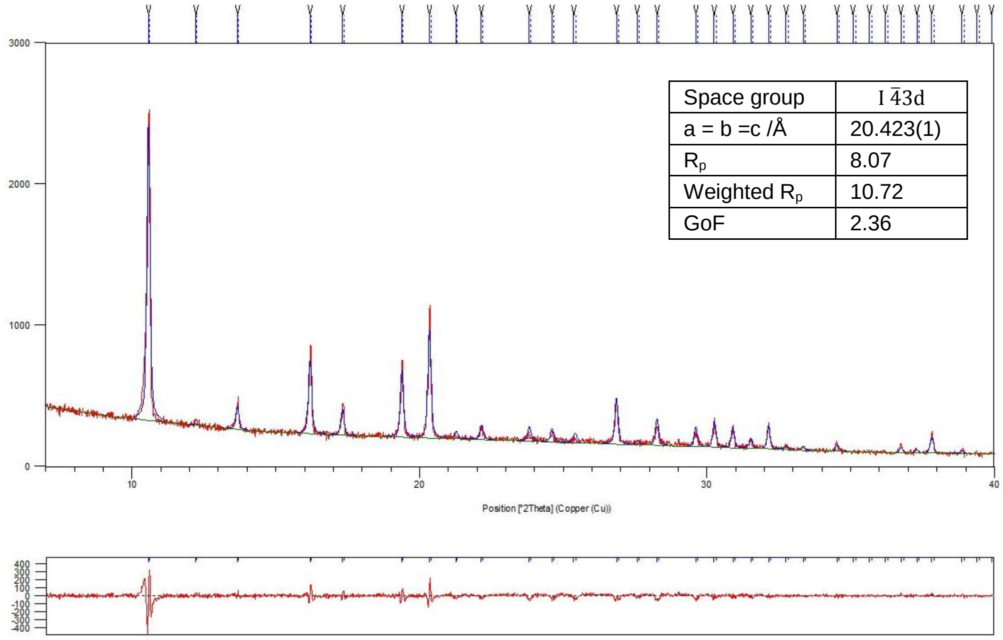

Space group	$I\bar{4}3d$
a = b =c /Å	20.423(1)
R_p	8.07
Weighted R_p	10.72
GoF	2.36

Figure S9. Le Bail fitting of PXRD pattern for $[TEA]_3[In_3(BTC)_4]$ after soaking in CH_2Cl_2. Experimental pattern (red), calculated pattern (blue), difference pattern expt-calc (bottom). Unit cell dimensions determined from the fit and agreement indices are listed in the inset.

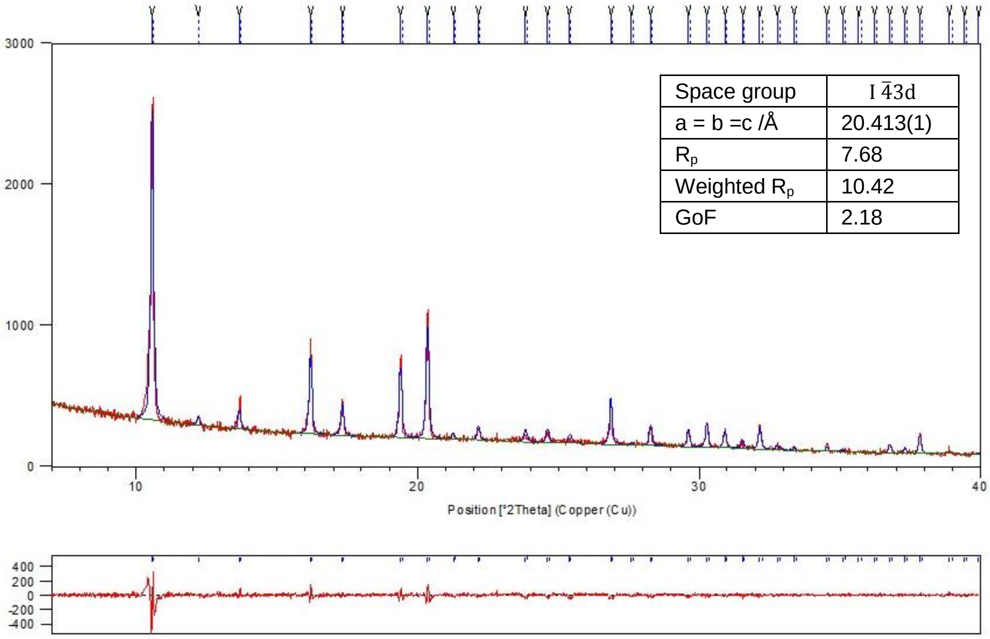

Space group	$I\bar{4}3d$
a = b =c /Å	20.413(1)
R_p	7.68
Weighted R_p	10.42
GoF	2.18

Figure S10 Le Bail fitting of PXRD pattern for $[TEA]_3[In_3(BTC)_4]$ after soaking in acetone. Experimental pattern (red), calculated pattern (blue), difference pattern expt-calc (bottom). Unit cell dimensions determined from the fit and agreement indices are listed in the inset.

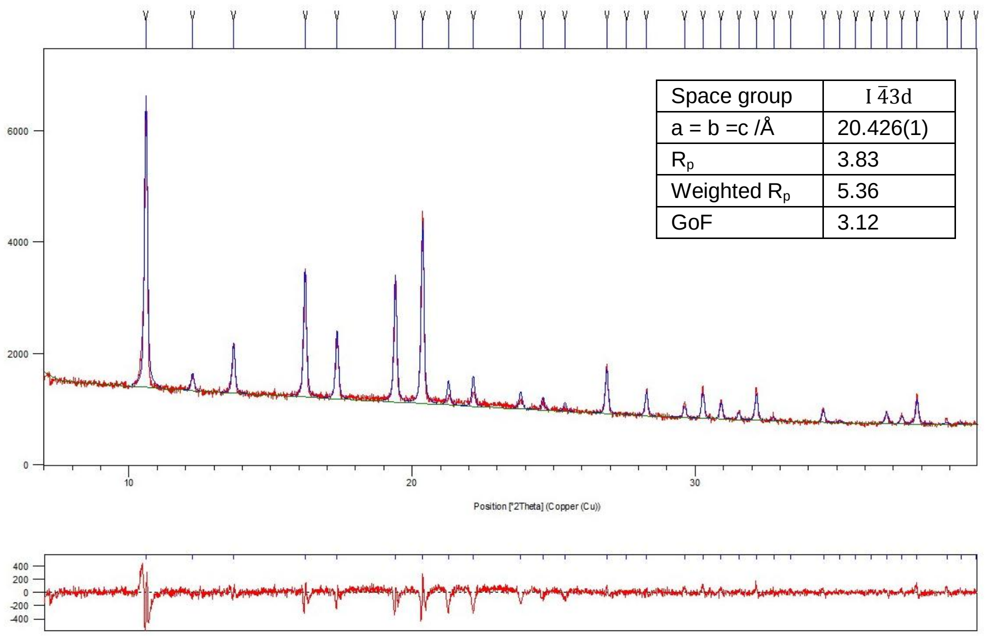

Space group	$I\bar{4}3d$
a = b =c /Å	20.426(1)
R_p	3.83
Weighted R_p	5.36
GoF	3.12

Figure S11. Le Bail fitting of PXRD pattern for $[(Cp_2Co)_x(TEA)_{3-x}][In_3(BTC)_4]$ (cation exchange in acetone for 24 h, initial molar ratio $[Cp_2Co]^+$/TEA = 3/1). Experimental pattern (red), calculated pattern (blue), difference pattern expt-calc (bottom). Unit cell dimensions determined from the fit and agreement indices are listed in the inset.

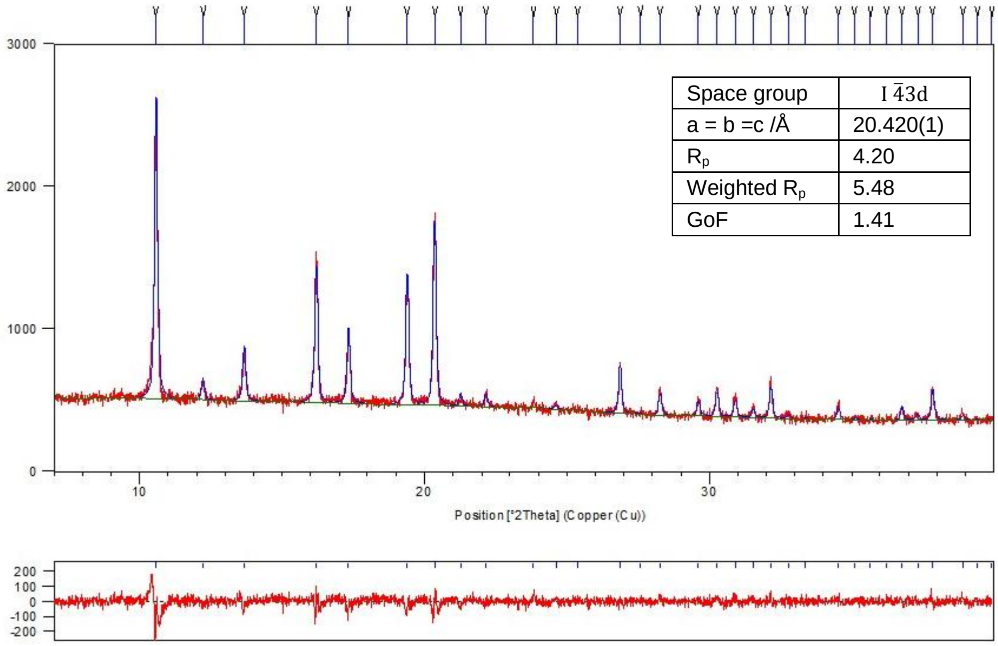

Space group	$I\bar{4}3d$
a = b =c /Å	20.420(1)
R_p	4.20
Weighted R_p	5.48
GoF	1.41

Figure S12. Le Bail fitting of PXRD pattern for $[(Cp_2Co)_x(TEA)_{3-x}][In_3(BTC)_4]$ (cation exchange in acetone for 48 h, initial $[Cp_2Co]^+$/TEA = 3/1). Experimental pattern (red), calculated pattern (blue), difference pattern expt-calc (bottom). Unit cell dimensions determined from the fit and agreement indices are listed in the inset.

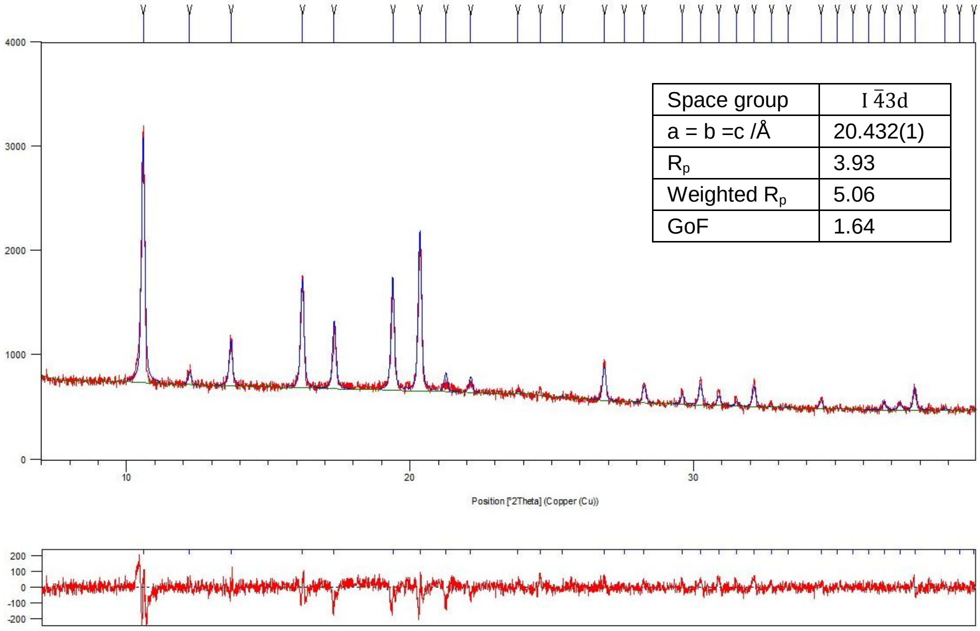

Space group	$I\bar{4}3d$
a = b =c /Å	20.432(1)
R_p	3.93
Weighted R_p	5.06
GoF	1.64

Figure S13. Le Bail fitting of PXRD pattern for $[(Cp_2Co)_x(TEA)_{3-x}][In_3(BTC)_4]$ (cation exchange in acetone for 72 h, initial $[Cp_2Co]^+$/TEA = 3/1). Experimental pattern (red), calculated pattern (blue), difference pattern expt-calc (bottom). Unit cell dimensions determined from the fit and agreement indices are listed in the inset.

^{1}H NMR spectrum of $[Cp_2Co][PF_6]$ in DCl/d^6-dmso

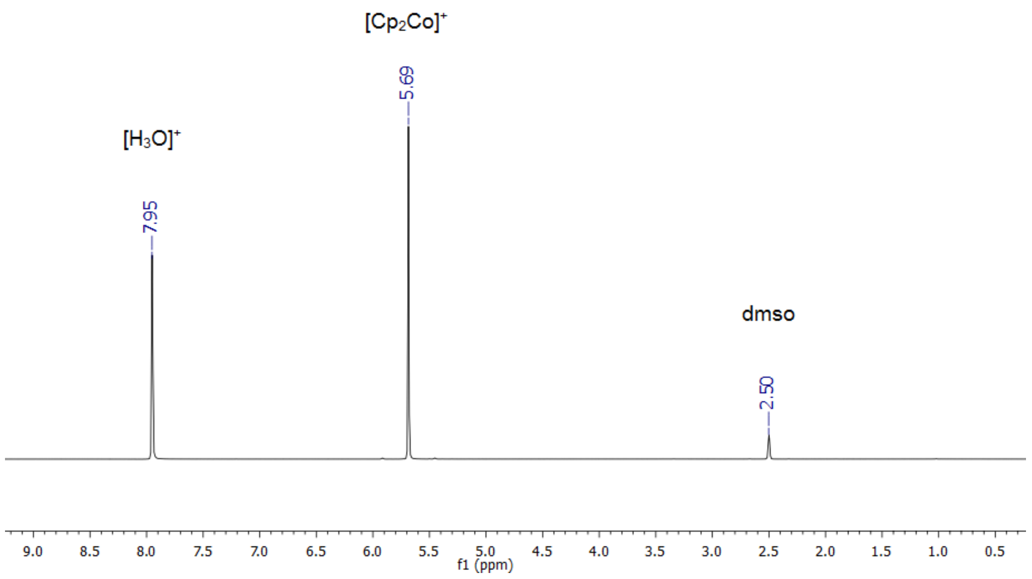

^{31}P NMR spectrum of $[Cp_2Co][PF_6]$ in DCl/d^6-dmso

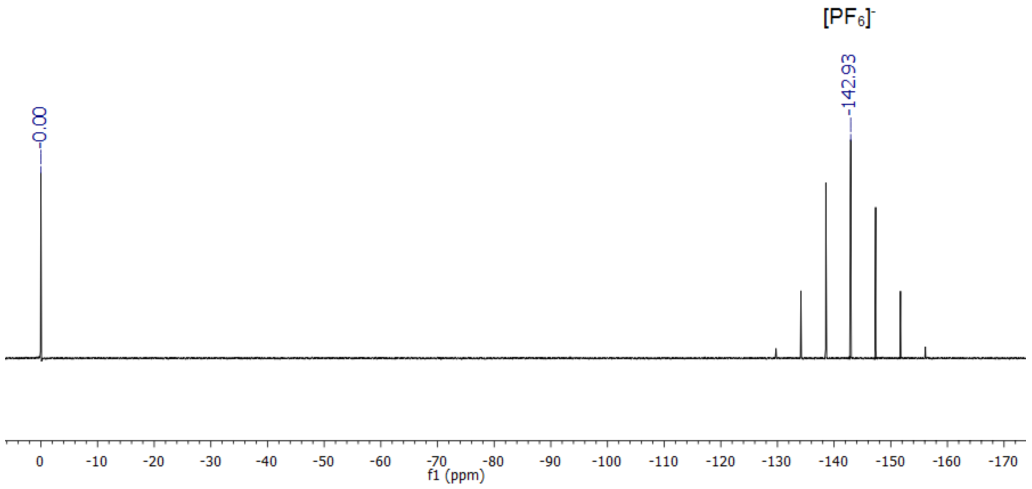

Figure S14. ^{1}H (top) and $^{31}P\{^1H\}$ (bottom) NMR spectrum of $[Cp_2Co][PF_6]$ in DCl/dmso-d^6. The septet at δ_P = -142.9 ppm is not observed in the $^{31}P\{^1H\}$ NMR spectrum of partially exchanged $[(Cp_2Co)_x(TEA)_{3-x}][In_3(BTC)_4]$, suggesting that only the $[Cp_2Co]^+$ cation is encapsulated.

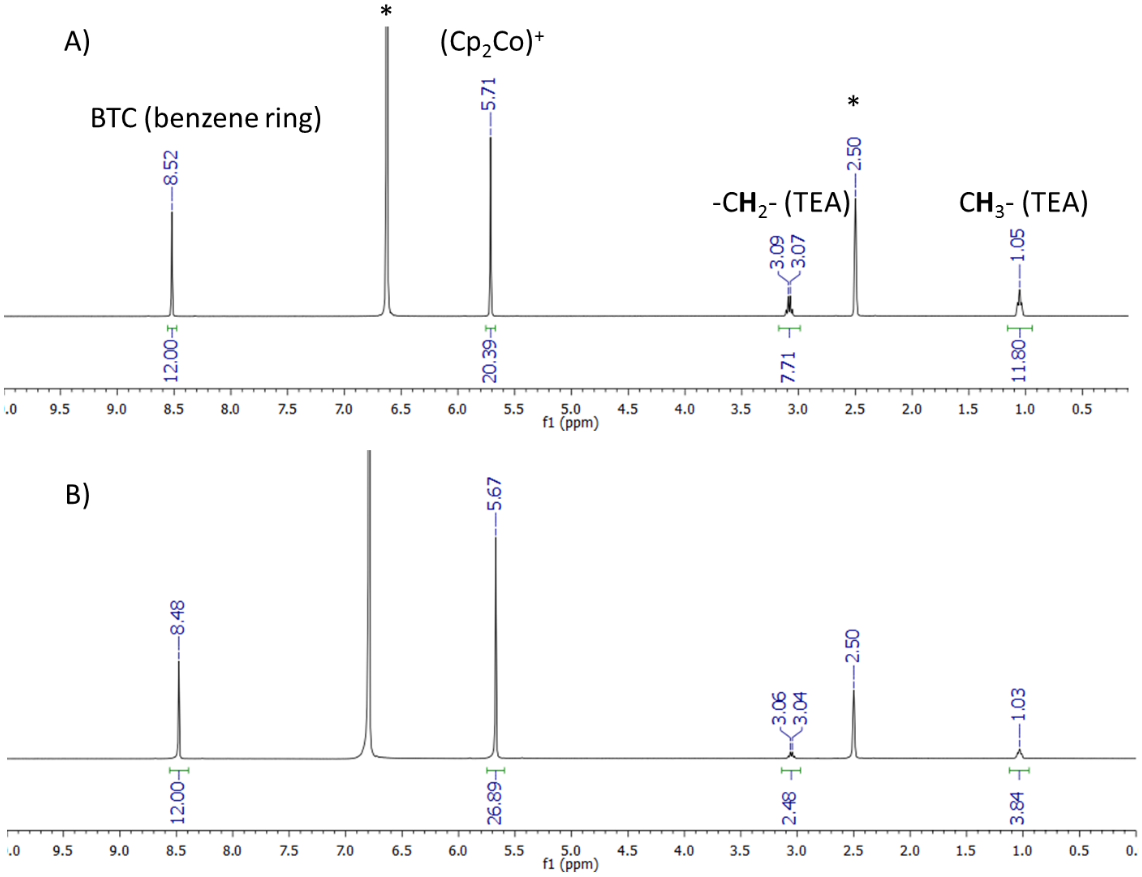

Figure S15. A) ^{1}H NMR of [$(Cp_2Co)_x(TEA)_{3-x}$][$In_3(BTC)_4$] in DCl/dmso-d^6 (1/5 v/v) after 3 days of exchange (initial [Cp_2Co]$^+$/TEA = 1/1). Integration of the respective peaks suggests approximately 68% (x = 2.04) cation exchange ([BTC: 12H], [Cp: 20.4H, x = 20.4/10 = 2.04], [CH_2: 7.7 H, x = 3-(7.7/8) = 2.04], [CH_3: 11.8 H, x = 3-(11.8/12) = 2.02]. B) ^{1}H NMR of [$(Cp_2Co)_x(TEA)_{3-x}$][$In_3(BTC)_4$] in DCl/dmso-d^6 (1/5 v/v) after 3 days of exchange (initial [Cp_2Co]$^+$/TEA = 3/1). Integration of the respective peaks suggests approximately 90% (x = 2.69) cation exchange ([BTC: 12H], [Cp: 26.9H, x = 26.9/10 = 2.69], [CH_2: 2.5 H, x = 3-(2.5/8) = 2.69], [CH_3: 3.8 H, x = 3-(3.8/12) = 2.68]. NMR solvents are marked with an asterisk.

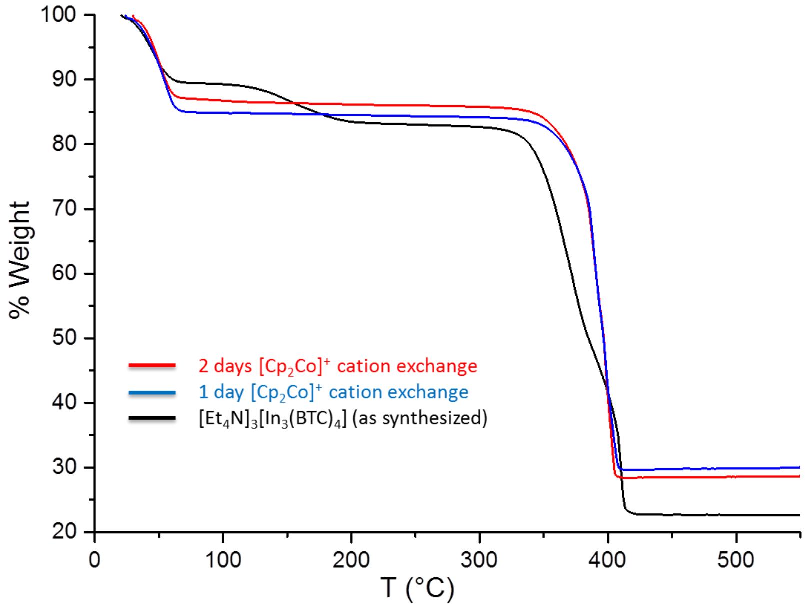

Figure S16. TGA of $[TEA]_3[In_3(BTC)_4]$ (black) and $[(Cp_2Co)_x(TEA)_{3-x}][In_3(BTC)_4]$ after 1 (red) and 2 (blue) days of cation exchange in acetone (initial molar ratio $[Cp_2Co]^+$/TEA = 1/1), showing the increase of inorganic/organic ratio due to encapsulation of $[Cp_2Co]^+$.

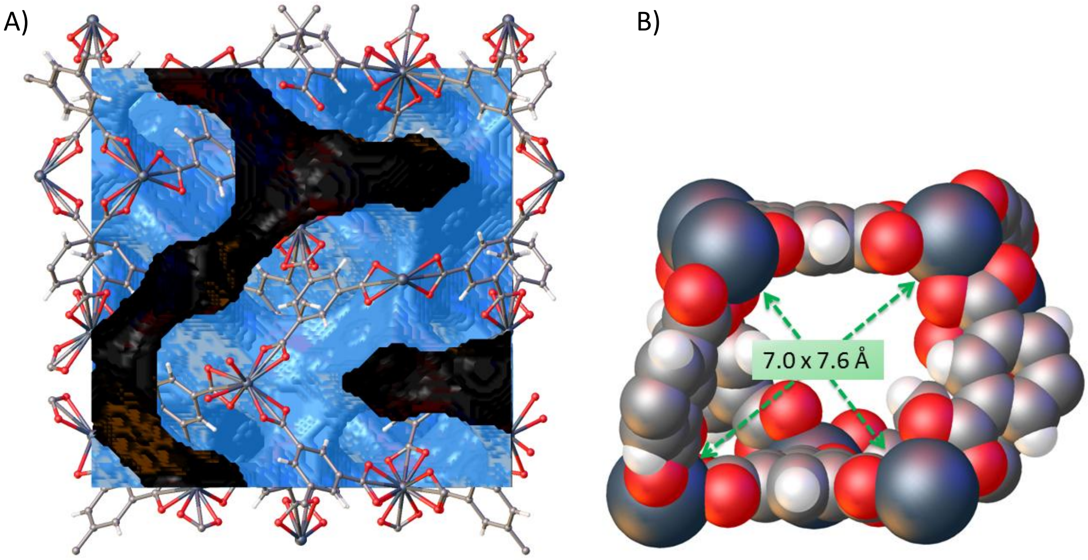

Figure S17. A) Single crystal structure of $[TEA]_3[In_3(BTC)_4]$[7] showing the calculated guest-accessible void space without any cations present (66% of the unit cell volume). B) Pore window defined by the BTC benzene rings. Distances listed, corrected for van der Waals radii, correspond to In–C_{ortho} (7.61 Å) and O–$C_{carboxylate}$ (7.03 Å) located on opposite corners of the window.

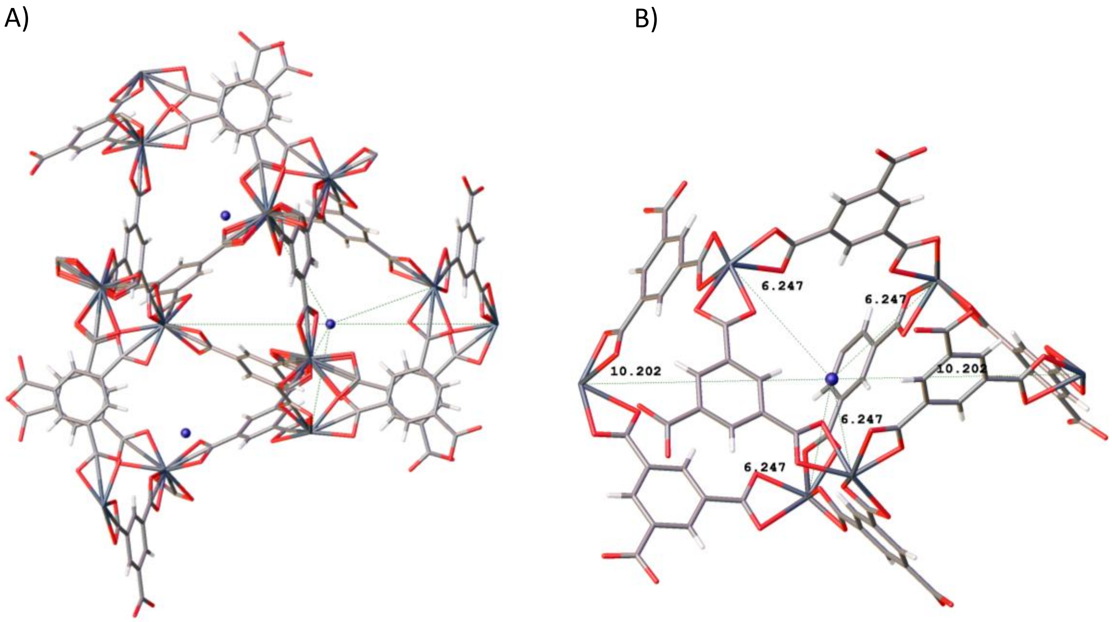

Figure S18. A) Single crystal structure of $[(Cp_2Co)_x(TEA)_{3-x}][In_3(BTC)_4]$. Only the cobalt atoms (blue spheres) of the $[Cp_2Co]^+$ cations can be reliably modelled, positioned on the $\bar{4}$ axes in the centre of the pores. B) Each cavity is defined by six tetrahedral $[In(O_2CR)_4]^-$ with the respective Co-In distances represented by green dotted lines.

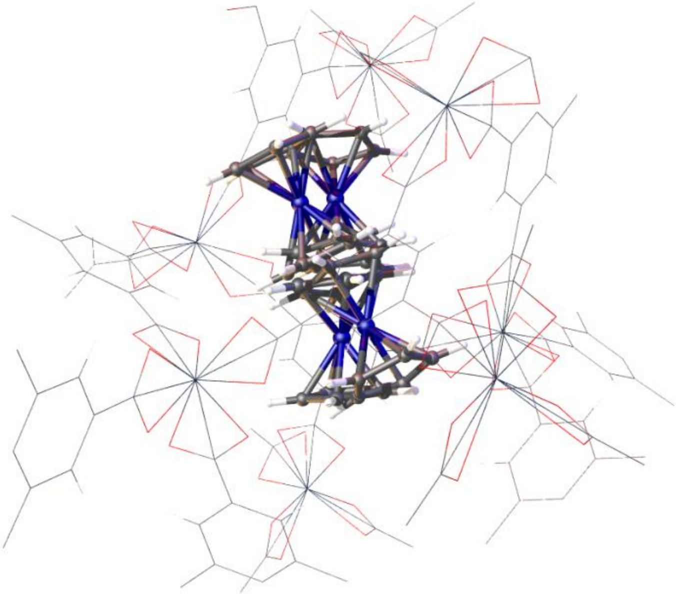

Figure S19. Single crystal structure of $[Cp_2Co]_3[In_3(BTC)_4]$ showing the disordered cations, located on four equivalent sites generated by a $\bar{4}$ axis.

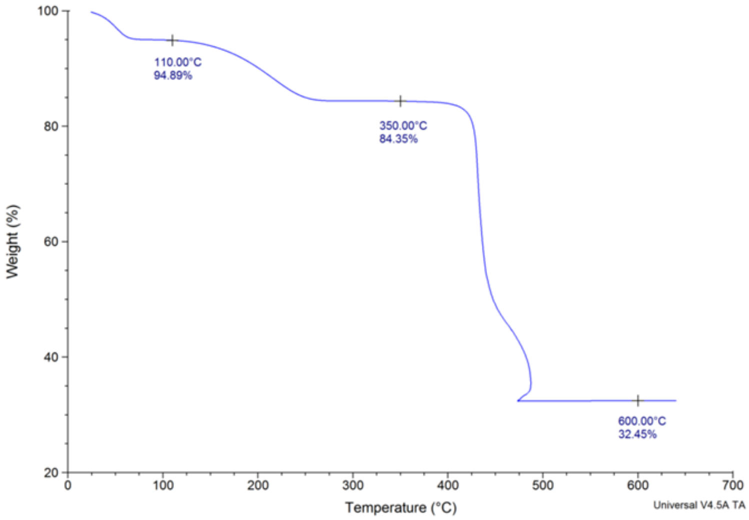

Figure S20. TGA curve of $[Cp_2Co]_3[In_3(BTC)_4].3(DMF).6(H_2O)$ showing the expected weight loss for H_2O (5.1%) and DMF (10.5%) evaporation.

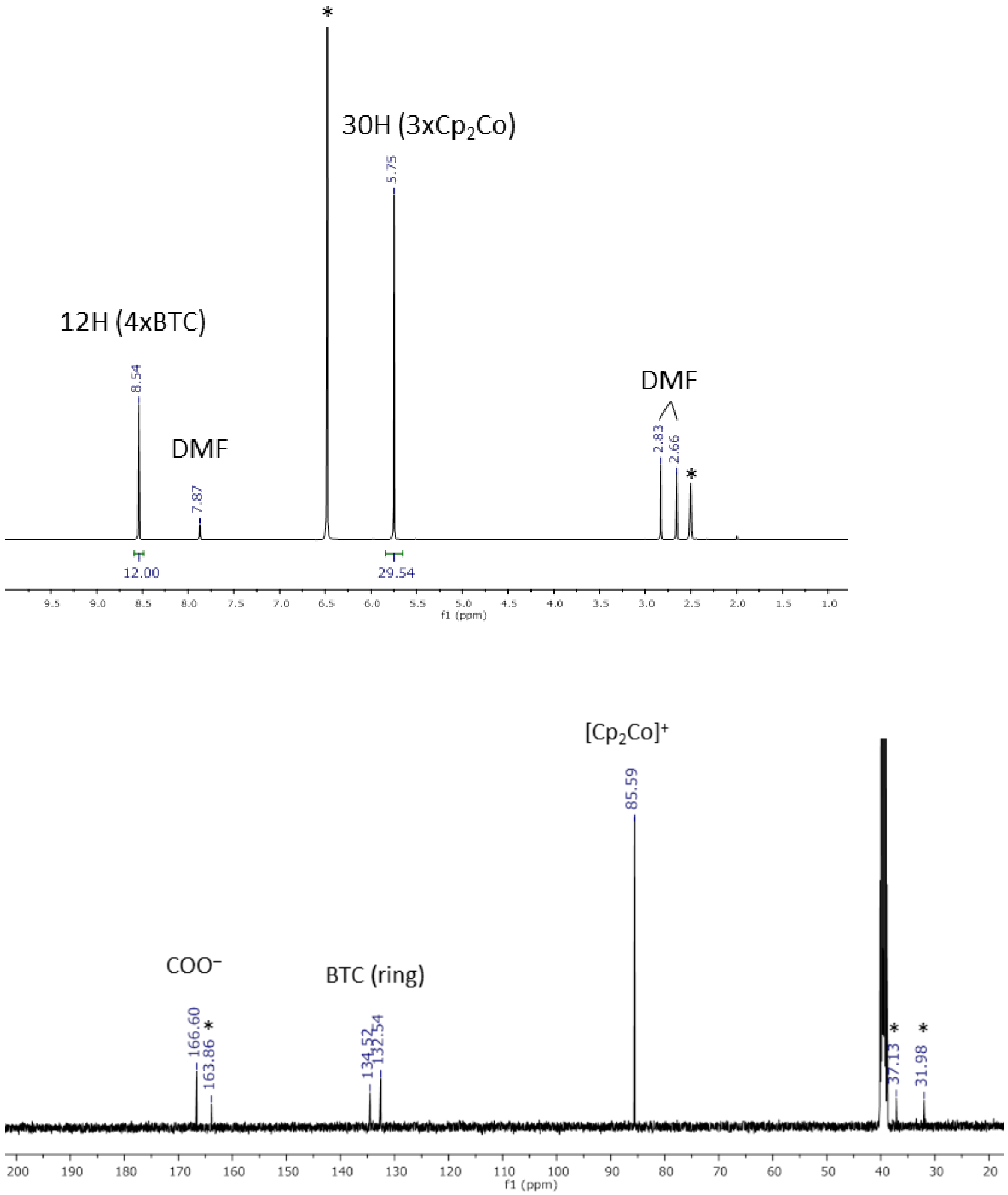

Figure S21. A) ^{1}H NMR of $[Cp_2Co]_3[In_3(BTC)_4].3(DMF).6(H_2O)$ after digestion in DCl/d^6-dmso (1/5 v/v). NMR solvent peaks are marked with an asterisk. B) ^{13}C NMR of the same compound after digestion in DCl/d^6-dmso (1/5 v/v). Peaks assigned to DMF trapped inside the pores are marked with an asterisk.

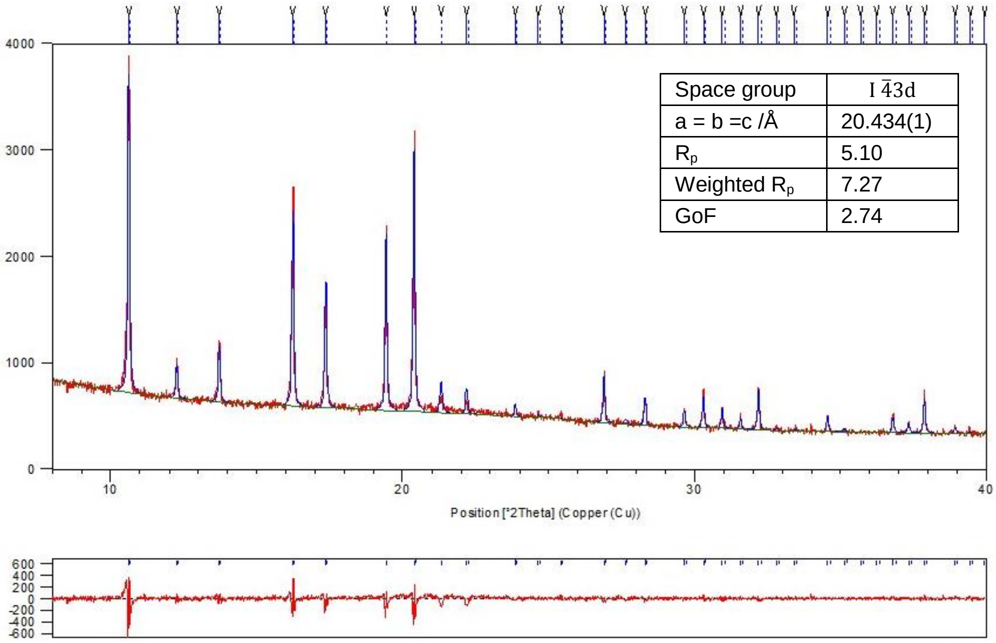

Space group	$I\bar{4}3d$
a = b =c /Å	20.434(1)
R_p	5.10
Weighted R_p	7.27
GoF	2.74

Figure S22. Le Bail fitting of PXRD pattern for as synthesized $[Cp_2Co]_3[In_3(BTC)_4]$. Experimental pattern (red), calculated pattern (blue), difference pattern expt-calc (bottom). Unit cell dimensions determined from the fit and agreement indices are listed in the inset.

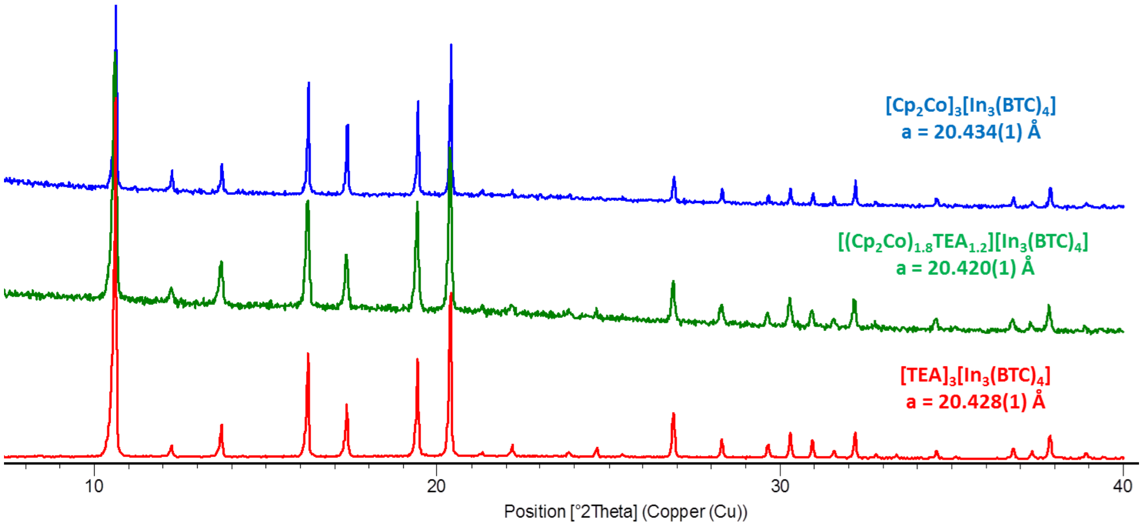

Figure S23. PXRD patterns of $[Cp_2Co]_3[In_3(BTC)_4]$ (blue), $[(Cp_2Co)_{1.8}(TEA)_{1.2}][In_3(BTC)_4]$ (green) and $[TEA]_3[In_3(BTC)_4]$ (red) along with calculated dimensions of the cubic unit cell after LeBail refinement. All patterns are refined using the same space group ($I\bar{4}3d$).

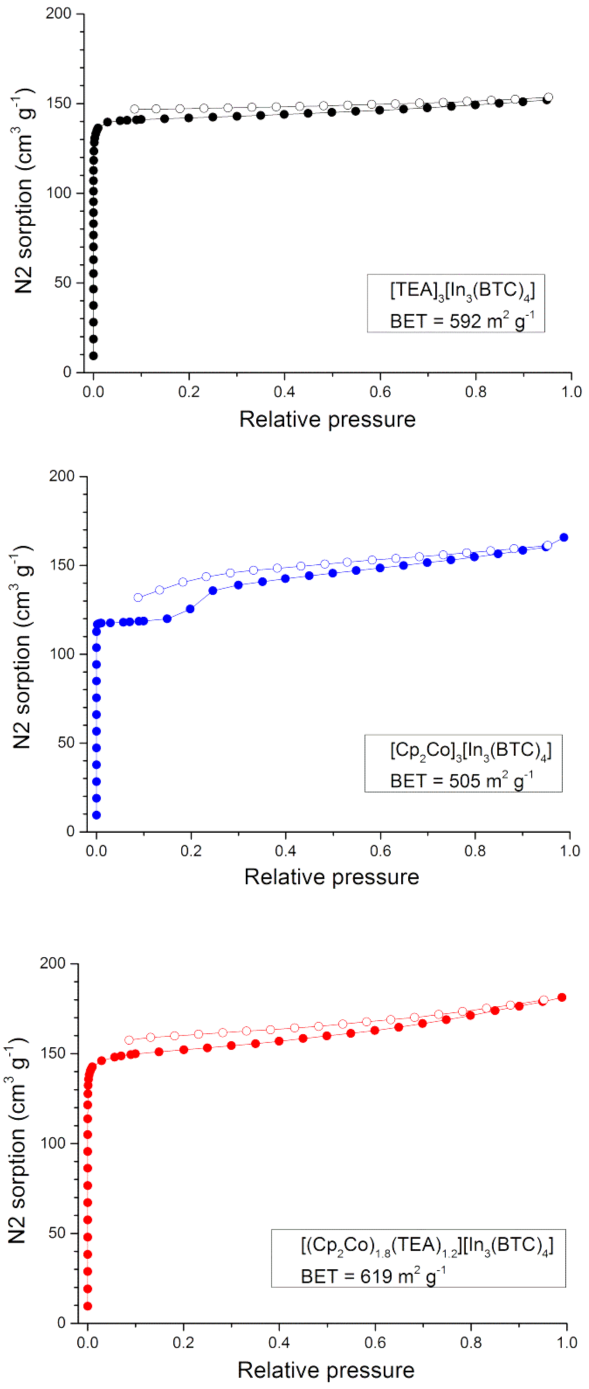

Figure S24. N_2 adsorption (filled circles) and desorption (empty circles) isotherms at 77 K for [TEA]$_3$[In$_3$(BTC)$_4$] (black), [Cp$_2$Co]$_3$[In$_3$(BTC)$_4$] (blue) and [(Cp$_2$Co)$_{1.8}$(TEA)$_{1.2}$][In$_3$(BTC)$_4$] (red). Activation: Solvent exchange in acetone for 24 h followed by high vacuum at 25 °C for 20 h.

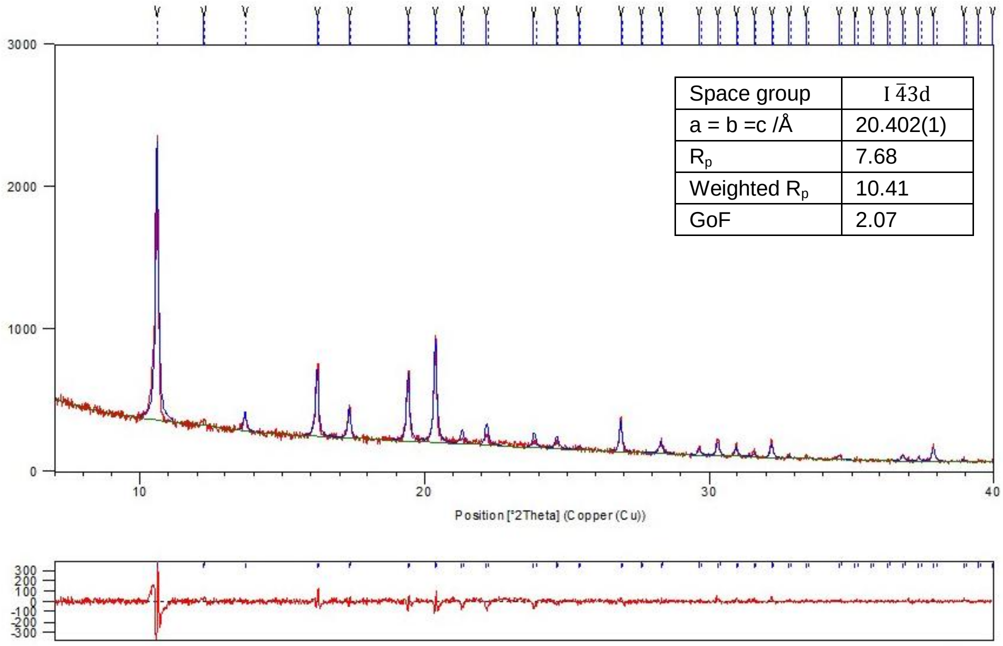

Space group	$I\bar{4}3d$
a = b =c /Å	20.402(1)
R_p	7.68
Weighted R_p	10.41
GoF	2.07

Figure S25. Le Bail fitting of PXRD pattern for $[TEA]_3[In_3(BTC)_4]$ after activation (solvent exchange in acetone for 24 h and high vacuum at 25 °C for 20 h). Experimental pattern (red), calculated pattern (blue), difference pattern expt-calc (bottom). Unit cell dimensions determined from the fit and agreement indices are listed in the inset.

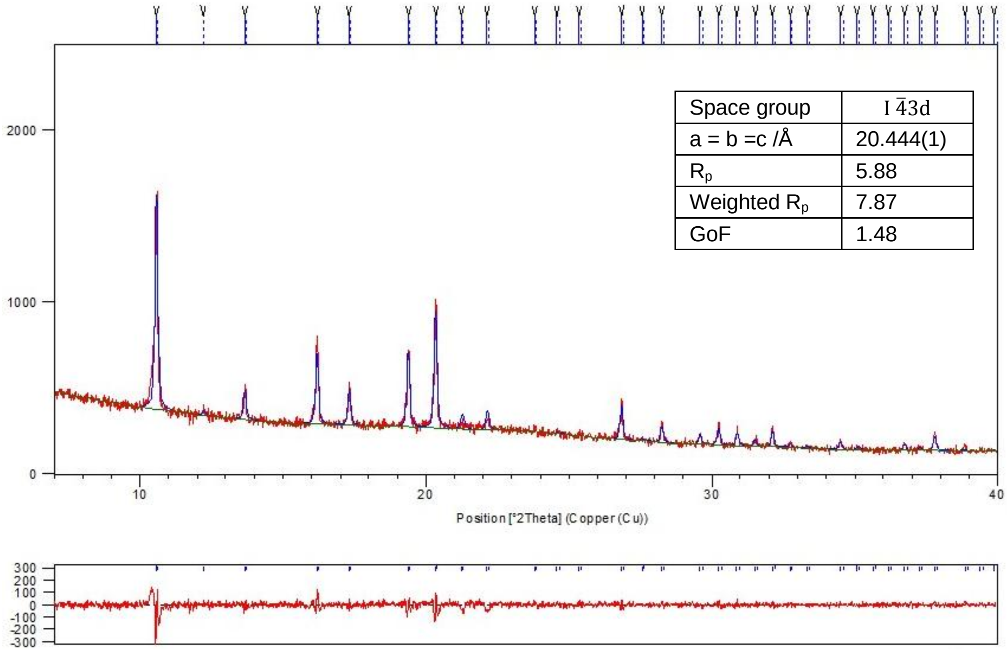

Space group	$I\bar{4}3d$
a = b =c /Å	20.444(1)
R_p	5.88
Weighted R_p	7.87
GoF	1.48

Figure S26. Le Bail fitting of PXRD pattern for $[(Cp_2Co)_{1.8}(TEA)_{1.2}][In_3(BTC)_4]$ after activation (solvent exchange in acetone for 24 h and high vacuum at 25 °C for 20 h). Experimental pattern (red), calculated pattern (blue), difference pattern expt-calc (bottom). Unit cell dimensions determined from the fit and agreement indices are listed in the inset.

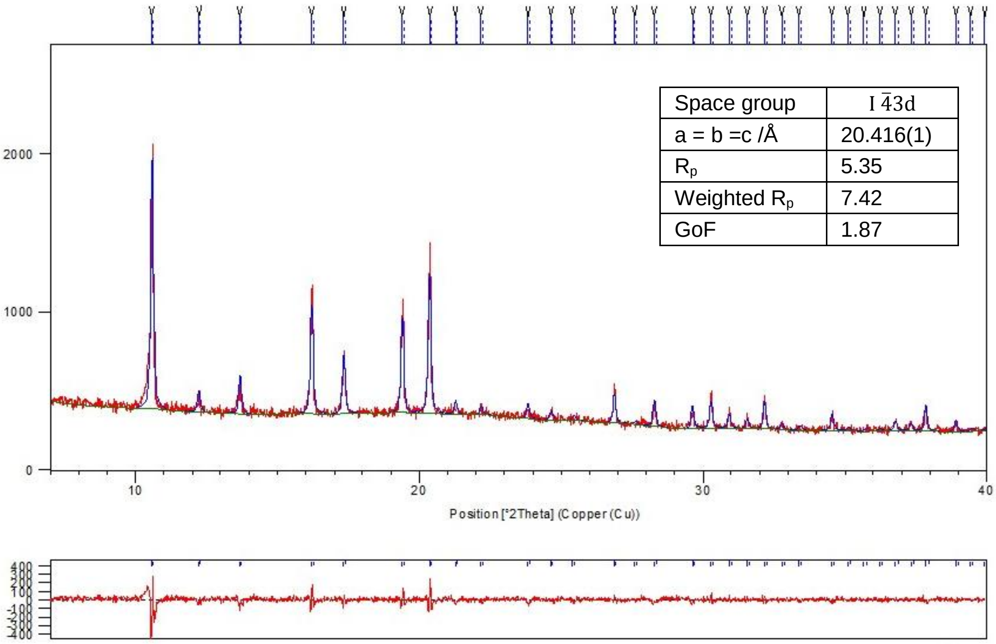

Space group	$I\bar{4}3d$
a = b =c /Å	20.416(1)
R_p	5.35
Weighted R_p	7.42
GoF	1.87

Figure S27. Le Bail fitting of PXRD pattern for $[Cp_2Co]_3[In_3(BTC)_4]$ after activation (solvent exchange in acetone for 24 h and high vacuum at 25 °C for 20 h). Experimental pattern (red), calculated pattern (blue), difference pattern expt-calc (bottom). Unit cell dimensions determined from the fit and agreement indices are listed in the inset.

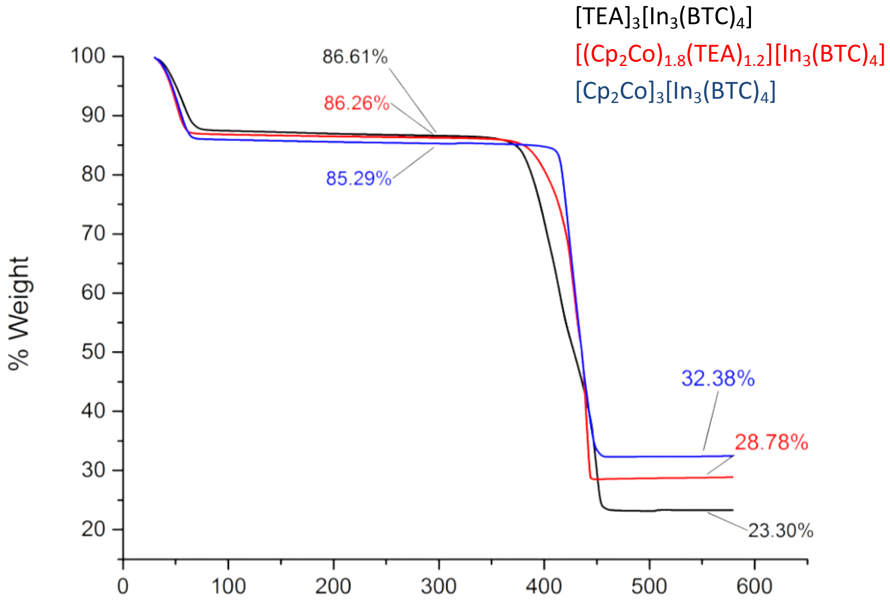

Figure S28. TGA curves after activation (solvent exchange in acetone for 24 h and high vacuum at RT for 20 h) for $[TEA]_3[In_3(BTC)_4]$ (black), $[(Cp_2Co)_{1.8}(TEA)_{1.2}][In_3(BTC)_4]$ (red) and $[Cp_2Co]_3[In_3(BTC)_4]$ (blue), showing the increase in inorganic/organic ratio due to encapsulation of $[Cp_2Co]^+$.

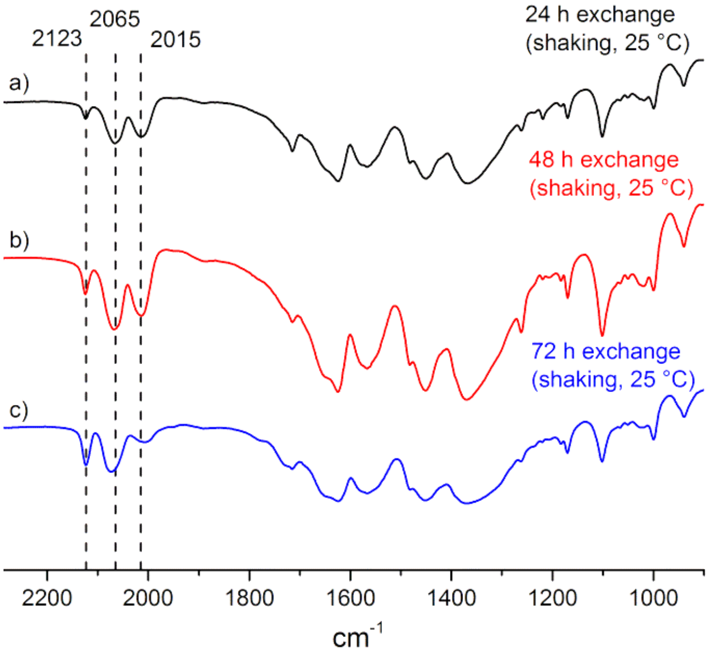

Figure S29. IR spectra of $[(Fp\text{-}L)_x(TEA)_{3-x}][In_3(BTC)_4]$ prepared by shaking for (a) 24 h (b) 48 h and (c) 72 h at 25 °C. Intensity of the high frequency band at 2123 cm^{-1} is increasing with time due to formation and simultaneous encapsulation of the tricarbonyl adduct $[Fp\text{-}CO]^+$ (along with $[Fp\text{-}L]^+$).

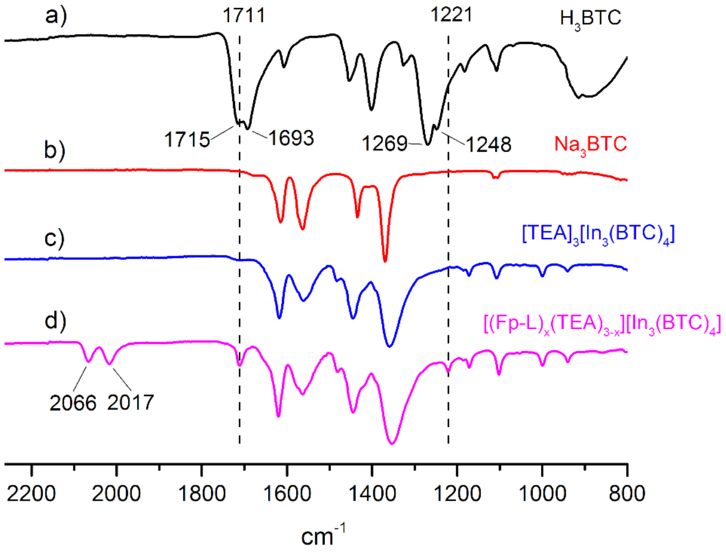

Figure S30. IR spectra of (a) H_3BTC (b) Na_3BTC (c) as synthesized $[TEA]_3[In_3(BTC)_4]$ and (d) as synthesized $[(Fp\text{-}L)_{0.6}(TEA)_{2.4}][In_3(BTC)_4]$. Two additional peaks at 1711 and 1221 cm^{-1} are observed for $[(Fp\text{-}L)_{0.6}(TEA)_{2.4}][In_3(BTC)_4]$ which can be tentatively assigned to acetone trapped inside the pores after cation exchange and not H_3BTC linker impurities.

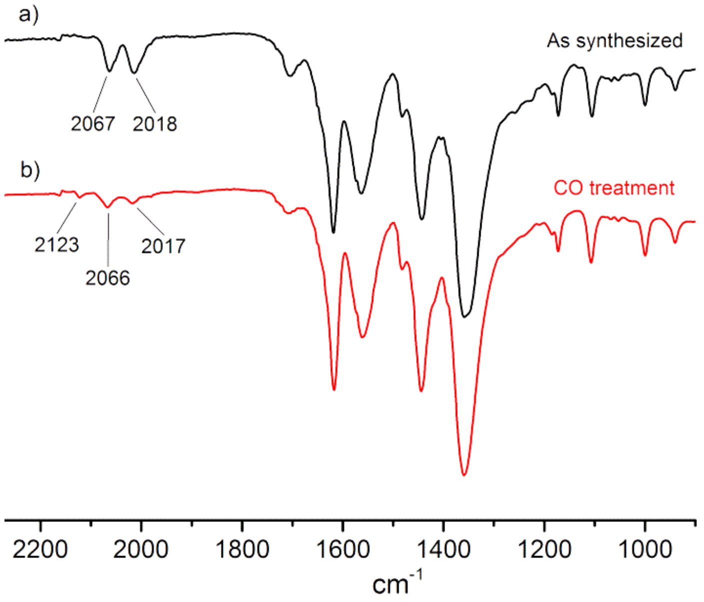

Figure S31. IR spectra of $[(Fp\text{-}L)_{0.6}(TEA)_{2.4}][In_3(BTC)_4]$ (a) as synthesized (soaking at 5 °C for 48 h) and (b) after treatment in the solid-state with CO gas for 15 min. Observation of the high frequency peak at 2123 cm^{-1} indicates formation of the tricarbonyl adduct $[Fp\text{-}CO]^+$ and confirms the presence of a labile site in the iron's coordination sphere.

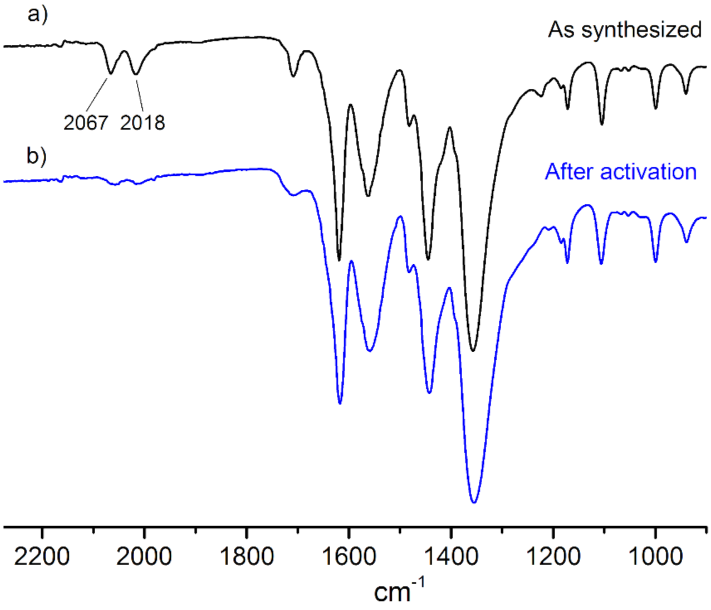

Figure S32. IR spectra of $[(Fp\text{-}L)_{0.6}(TEA)_{2.4}][In_3(BTC)_4]$ (a) as synthesized (soaking at 5 °C for 48 h) and (b) after attempt to remove solvent molecules (activation conditions: high vacuum at 25 °C for 20 h). Intensity of the *v*(CO) bands is dramatically decreased after activation, suggesting decomposition of the encapsulated $[Fp\text{-}L]^+$ cation via dissociation of the CO ligands.

$[TEA]_3[In_3(BTC)_4]$ as synthesized.

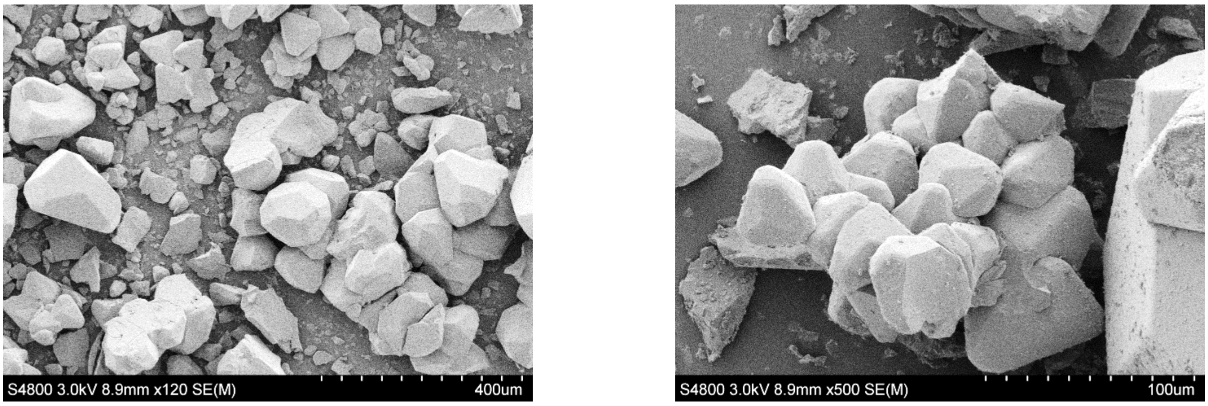

$[(Fp\text{-}L)_{0.6}(TEA)_{2.4}][In_3(BTC)_4]$ as synthesized.

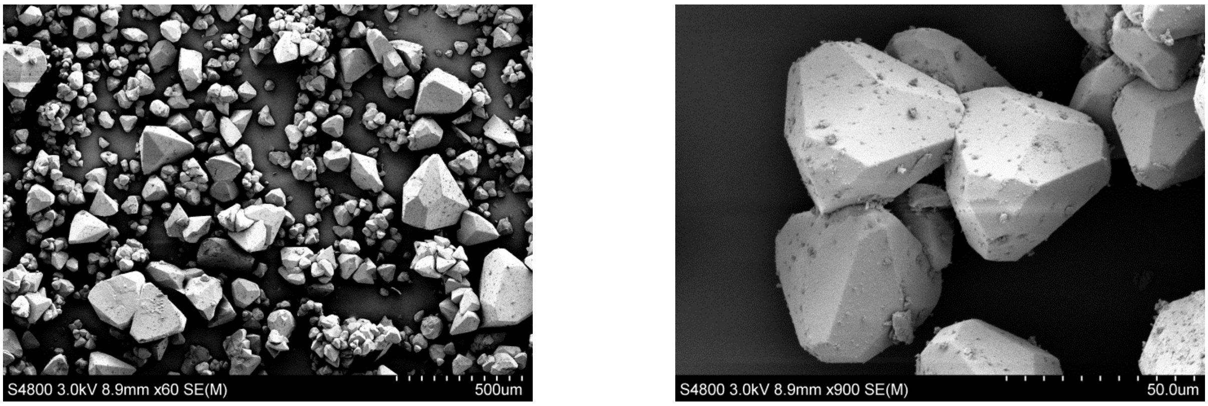

$[(Fp\text{-}L)_{0.6}(TEA)_{2.4}][In_3(BTC)_4]$ after one catalytic cycle.

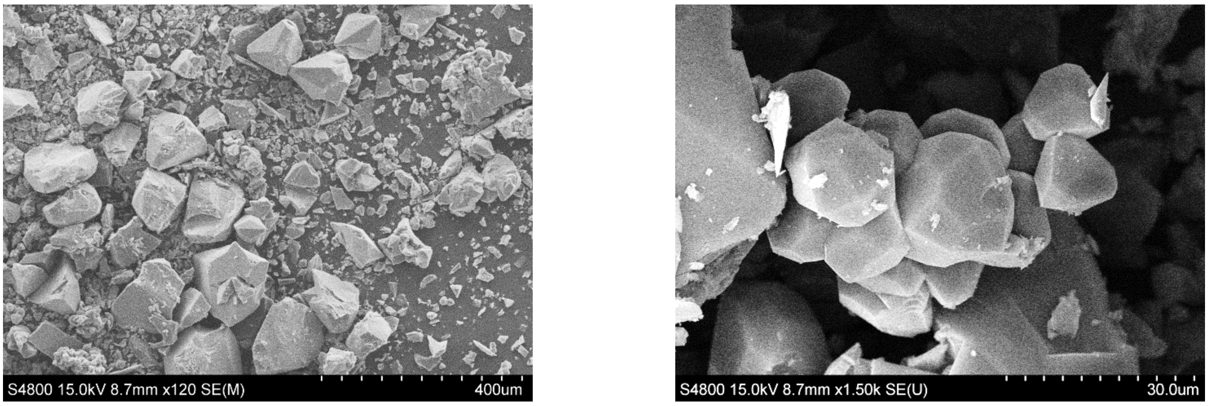

Figure S33. SEM images of as synthesized $[TEA]_3[In_3(BTC)_4]$ (top), $[(Fp\text{-}L)_{0.6}(TEA)_{2.4}][In_3(BTC)_4]$ as synthesized (middle) and after one catalytic cycle (bottom).

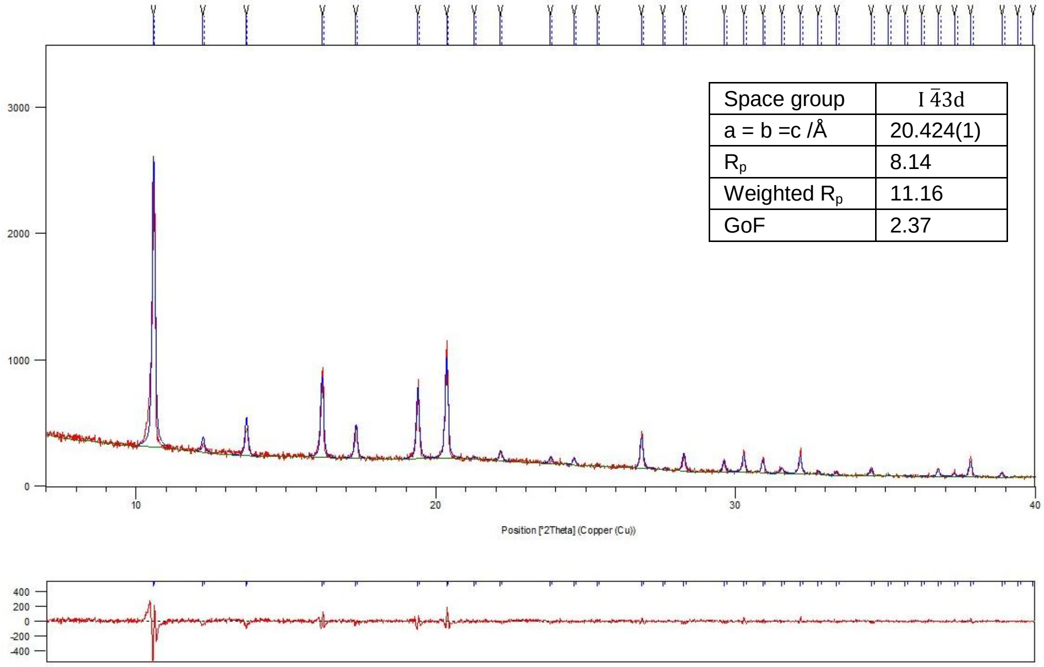

Space group	$I\bar{4}3d$
a = b =c /Å	20.424(1)
R_p	8.14
Weighted R_p	11.16
GoF	2.37

Figure S34. Le Bail fitting of PXRD pattern for as synthesized $[(Fp\text{-}L)_{0.6}(TEA)_{2.4}][In_3(BTC)_4]$. Experimental pattern (red), calculated pattern (blue), difference pattern expt-calc (bottom). Unit cell dimensions determined from the fit and agreement indices are listed in the inset.

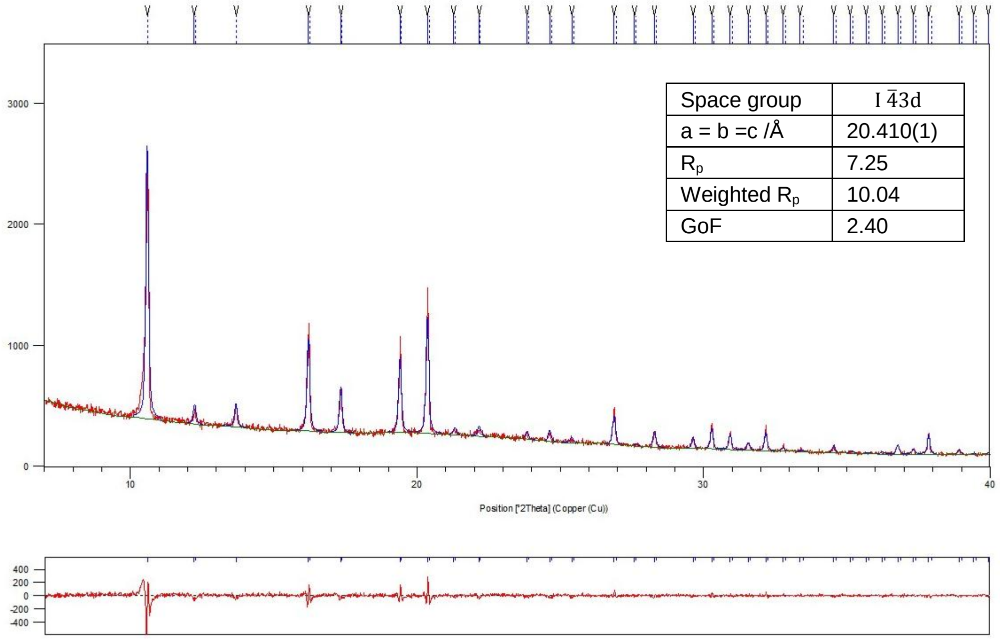

Space group	$I\bar{4}3d$
a = b =c /Å	20.410(1)
R_p	7.25
Weighted R_p	10.04
GoF	2.40

Figure S35. Le Bail fitting of PXRD pattern for $[(Fp\text{-}L)_{0.6}(TEA)_{2.4}][In_3(BTC)_4]$ recovered after one catalytic cycle. Experimental pattern (red), calculated pattern (blue), difference pattern expt-calc (bottom). Unit cell dimensions determined from the fit and agreement indices are listed in the inset.

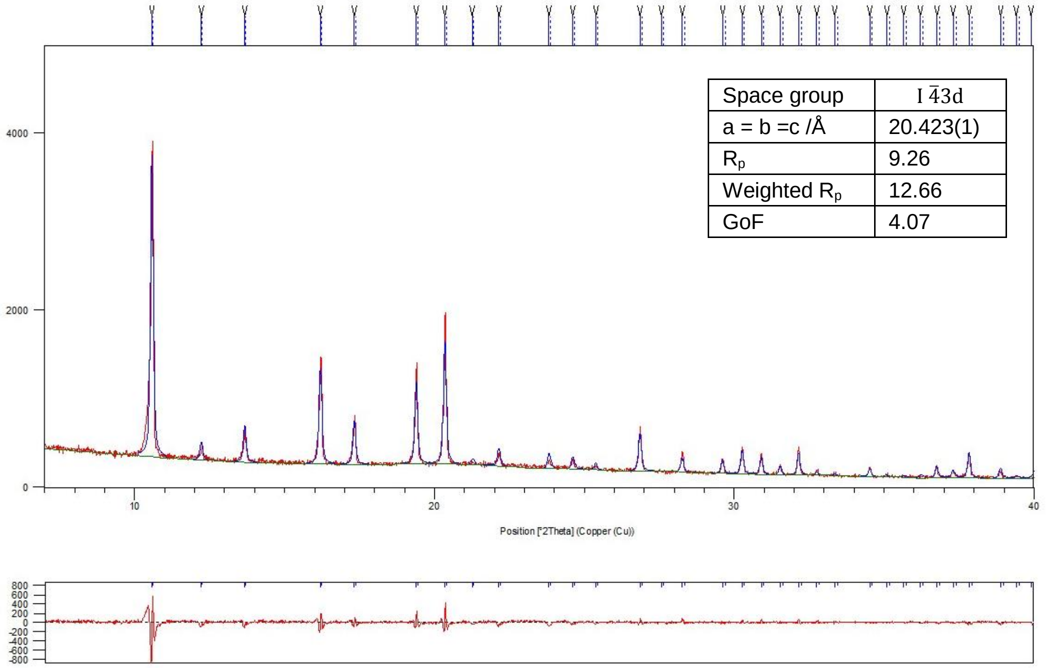

Space group	$I\bar{4}3d$
a = b =c /Å	20.423(1)
R_p	9.26
Weighted R_p	12.66
GoF	4.07

Figure S36. Le Bail fitting of PXRD pattern for $[(\text{Fp-L})_{0.6}(\text{TEA})_{2.4}][\text{In}_3(\text{BTC})_4]$ recovered after three catalytic cycles. Experimental pattern (red), calculated pattern (blue), difference pattern expt-calc (bottom). Unit cell dimensions determined from the fit and agreement indices are listed in the inset.

^{1}H NMR spectrum of [(Fp-THF)][BF$_4$] in DCl/d^6-dmso

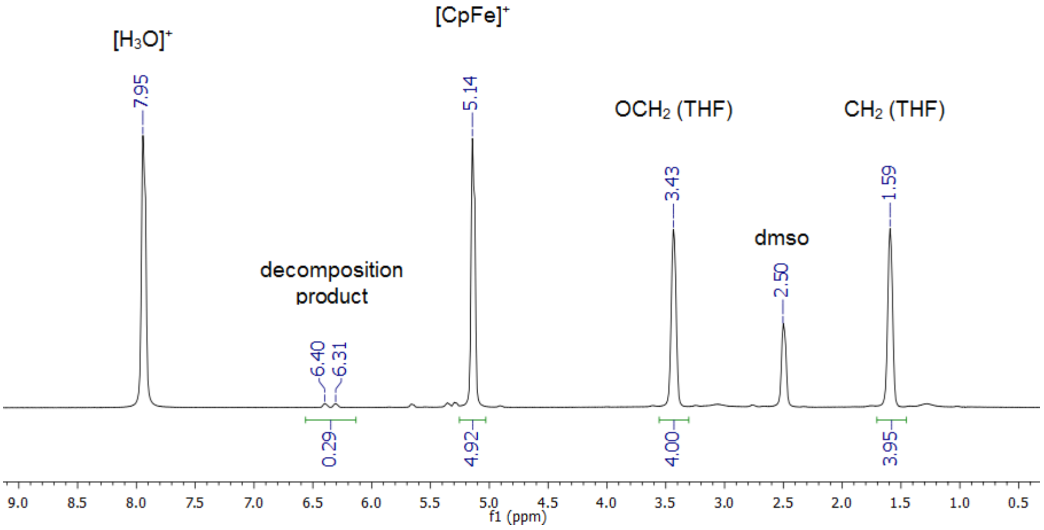

^{1}H NMR spectrum of [(Fp-THF)][BF$_4$] after 2 days in DCl/d^6-dmso

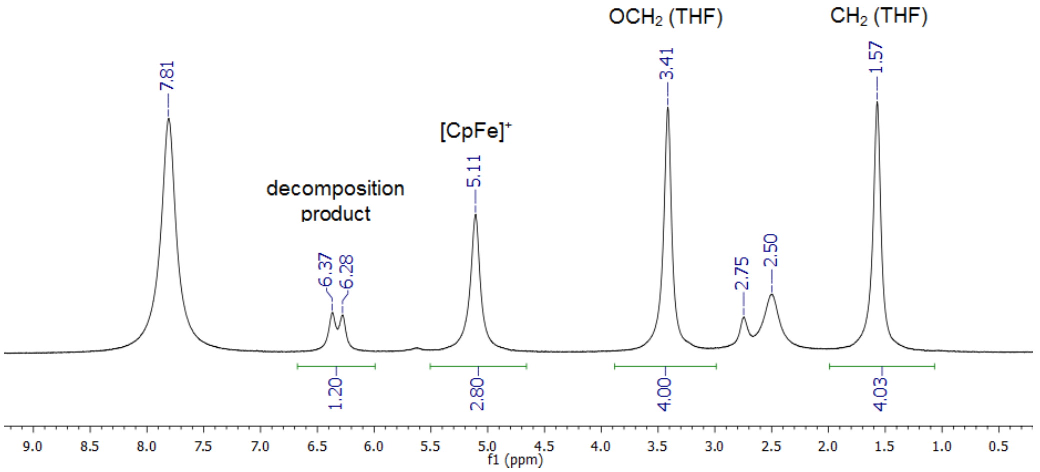

Figure S37. ^{1}H NMR spectrum of [(Fp-THF)][BF$_4$] in DCl/d^6-dmso (1/5 v/v) for t = 0 h (top) and t = 48 h (bottom). Decomposition is demonstrated by the relative change of intensities of the peaks at 5.1 ppm (singlet) and the lower field set of peaks at 6.3 ppm.

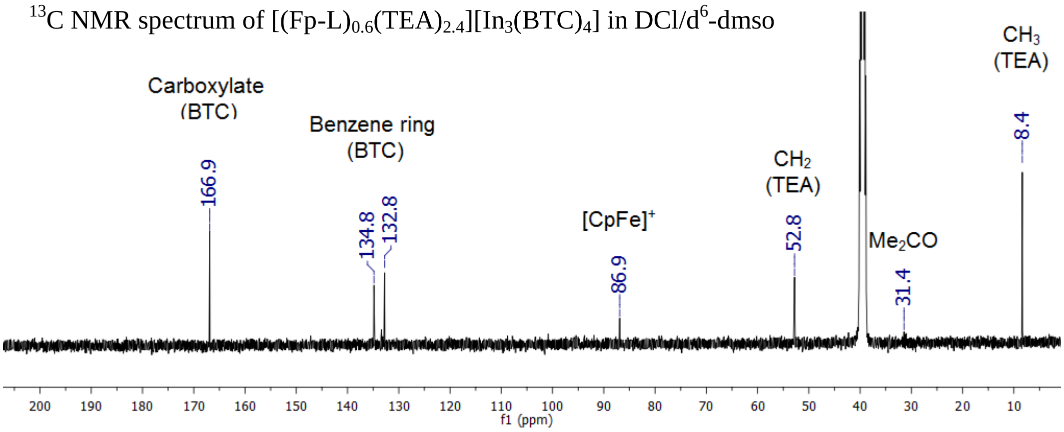

^{13}C NMR spectrum of $[(Fp\text{-}L)_{0.6}(TEA)_{2.4}][In_3(BTC)_4]$ in DCl/d^6-dmso

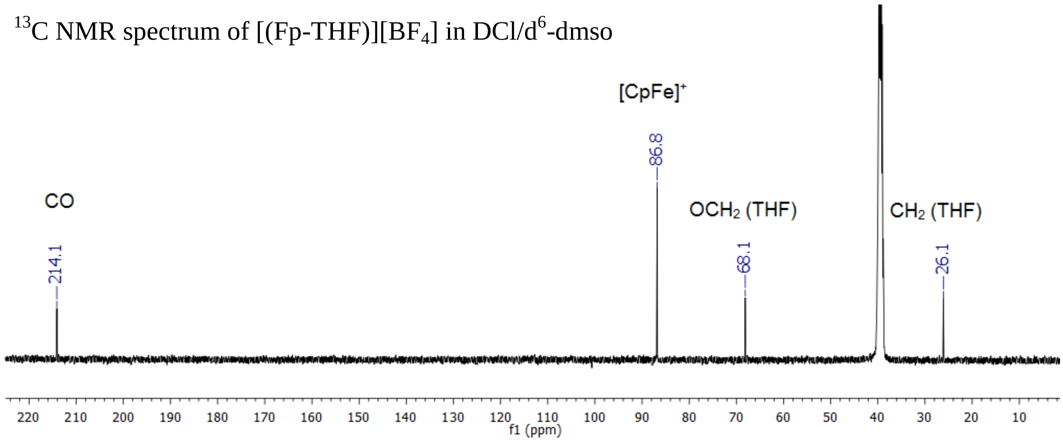

^{13}C NMR spectrum of $[(Fp\text{-}THF)][BF_4]$ in DCl/d^6-dmso

Figure S38. $^{13}C\{^1H\}$ NMR spectrum of $[(Fp\text{-}L)_{0.6}(TEA)_{2.4}][In_3(BTC)_4]$ (top) and $[(Fp\text{-}THF)][BF_4]$ (bottom) after digestion in DCl/d^6-dmso (1/5 v/v). Peaks due to THF are not observed in the ^{13}C spectrum of $[(Fp\text{-}L)_{0.6}(TEA)_{2.4}][In_3(BTC)_4]$, suggesting that L = acetone (solvent of exchange).

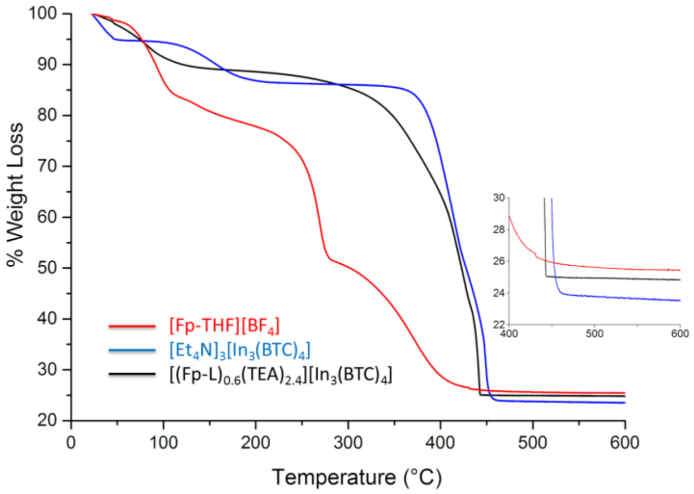

Figure S39. TGA curves of $[(Fp\text{-}L)_{0.6}(TEA)_{2.4}][In_3(BTC)_4]$ (black), $[TEA]_3[In_3(BTC)_4]$ (blue) and $[Fp\text{-}THF][BF_4]$ (red) showing the increase of inorganic residue for $[(Fp\text{-}L)_{0.6}(TEA)_{2.4}][In_3(BTC)_4]$ due to replacement of TEA by $[Fp\text{-}L]^+$ (inset) and a minor weight loss between 100 – 250 °C due to decomposition of $[Fp\text{-}L]^+$.

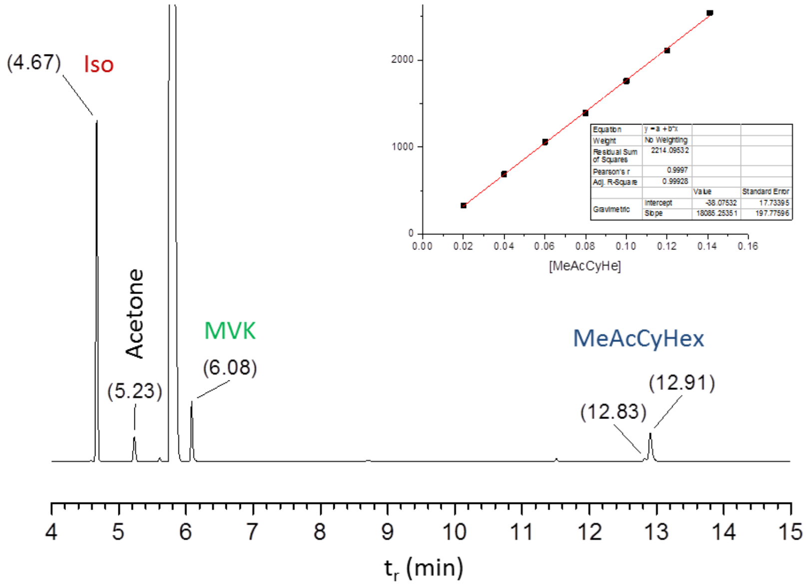

Equation	y = a + b*x		
Weight	No Weighting		
Residual Sum of Squares	2214.09532		
Pearson's r	0.9997		
Adj. R-Square	0.99928		
		Value	Standard Error
Gravimetric	Intercept	-38.07532	17.73395
	Slope	18085.25351	197.77596

Figure S40. GC analysis of the reaction mixture after heterogeneous Diels-Alder reaction. t_r = 4.67 : Isoprene, t_r = 5.23 : Acetone, t_r = 6.08 : MVK, t_r = 12.83 : 1-methyl-5-acetyl-cyclohexene (minor DA product), t_r = 12.91 : 1-methyl-4-acetyl-cyclohexene (major DA product). Calibration curve based on 1-methyl-4-acetyl-cyclohexene is shown in the inset.

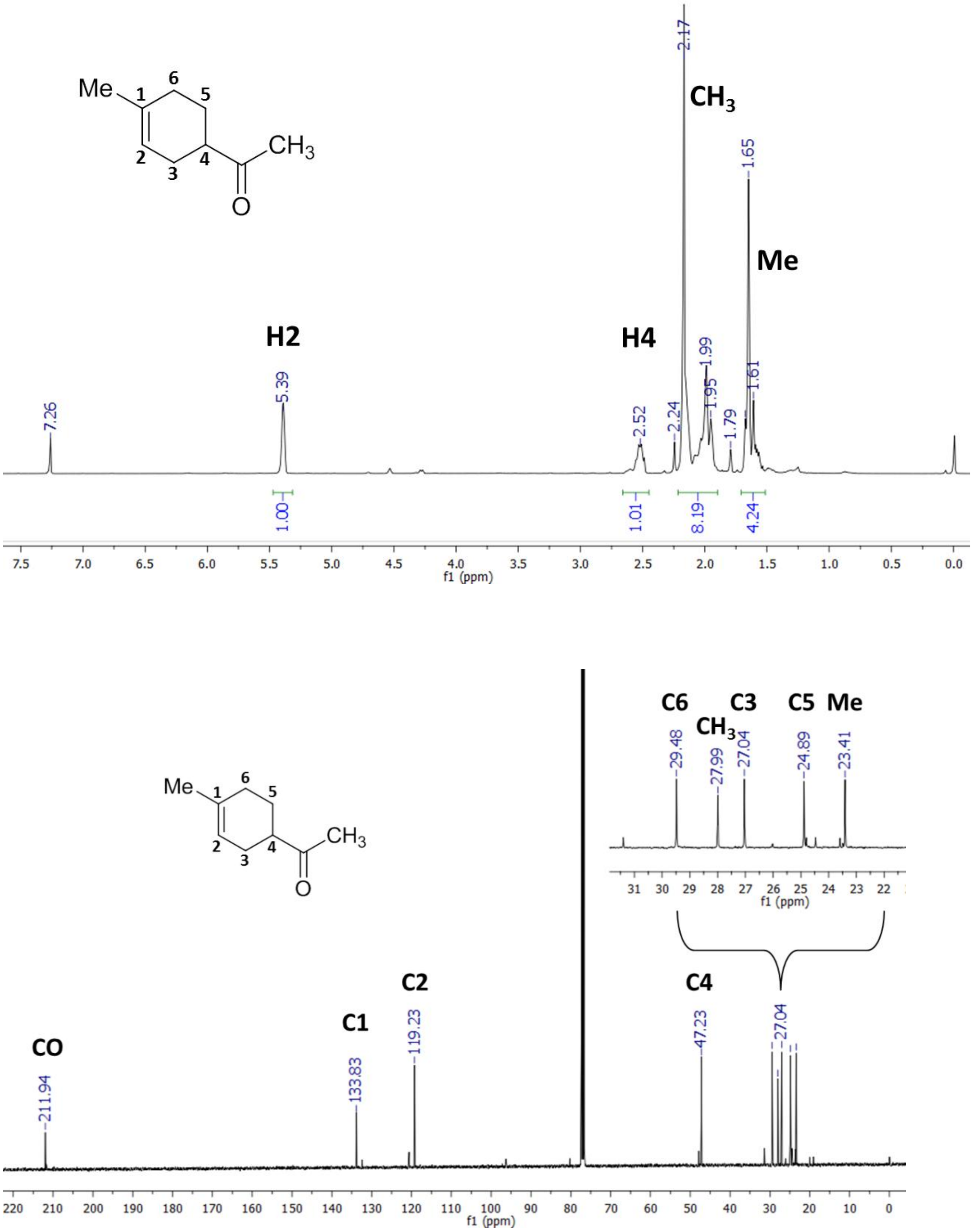

Figure S41. ^1H (top) and $^{13}C\{^1H\}$ NMR spectrum (bottom) of heterogeneous DA reaction mixture after removing all the volatile reactants, verifying the formation of 1-methyl-4-acetyl-cyclohexene. Peaks have been assigned by comparison with the respective spectra of the commercially available compound.

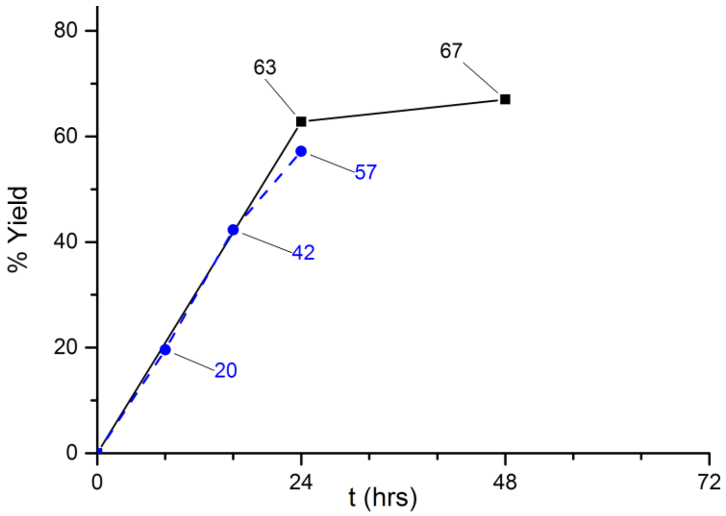

Figure S42. Yield *vs* time plot of the homogeneous DA reaction for shorter (blue) and longer (black) intervals under identical conditions (10% mol Fe/MVK in CH_2Cl_2, [Iso] = 0.4 M, [MVK] = 0.1 M).

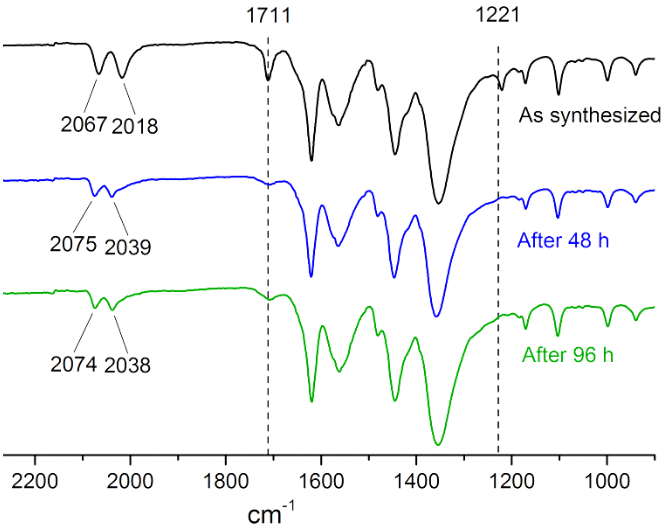

Figure S43. IR spectra of $[(Fp\text{-}L)_{0.6}(TEA)_{2.4}][In_3(BTC)_4]$ as synthesized (black), after 48 h DA reaction (red) and 96 h DA reaction. Spectra are normalized to the highest intensity peak. Shifting of the v(CO) peaks suggests that the coordination environment of the encapsulated catalyst is changing after turnover.

Table S1. $[Cp_2Co]^+$ cation exchange[a] for CPM-5 and $[R_4N]_3[In_3(BTC)_4]$ calculated by ICP-OES. Total exchange of organic cations by $[Cp_2Co]^+$ corresponds to 100% for a stoichiometrically controlled process.

$[Me_2NH_2][In_3(\mu\text{-}O)(BTC)_2(H_2O)_3]_2[In_3(BTC)_4] + x\ [Cp_2Co][PF_6] \rightarrow$ $[(Cp_2Co)_x(Me_2NH_2)_{1-x}][In_3(\mu\text{-}O)(BTC)_2(H_2O)_3]_2[In_3(BTC)_4] + x\ [Me_2NH_2][PF_6]$			
	24 h	72 h	120 h
CPM-5[b]	76%	111%	120%
$[R_4N]_3[In_3(BTC)_4] + x\ [Cp_2Co][PF_6] \rightarrow [(Cp_2Co)_x(R_4N)_{3-x}][In_3(BTC)_4] + x\ [R_4N]\ ][PF_6]$			
	24 h	48 h	72 h
$[Et_4N]_3[In_3(BTC)_4]$	53% (x = 1.59)	59% (x = 1.77)	60% (x = 1.80)
$[Pr_4N]_3[In_3(BTC)_4]$	29% (x = 0.87)	32% (x = 0.96)	36% (x = 1.08)
$[Bu_4N]_3[In_3(BTC)_4]$	7% (x = 0.21)	15% (x = 0.45)	16% (x = 0.48)

a) 0.02 M solution of $[Cp_2Co][PF_6]$ in acetone, 1/1 initial $[Cp_2Co]^+$/[organic cation]$^+$ ratio. b) Cation exchange formally exceeds 100%, suggesting that the $[Cp_2Co][PF_6]$ ion pair is also encapsulated.

Table S2. $[Cp_2Co]^+$ cation exchange[a] for $[Et_4N]_3[In_3(BTC)_4]$ calculated by ^{1}H NMR after digestion and ICP-OES for initial cation ratio $[Cp_2Co]^+/[Et_4N]^+$ = 3/1 or 1/1 (x = 3 corresponds to 100%).

$$[Et_4N]_3[In_3(BTC)_4] + x\ [Cp_2Co][PF_6] \rightarrow [(Cp_2Co)_x(Et_4N)_{3-x}][In_3(BTC)_4] + x\ [Et_4N][PF_6]$$

$[Cp_2Co]^+/[Et_4N]^+ = 3$[a]	24 h	48 h	72 h
% Cation Exchange (^{1}H NMR)[b]	68% (x = 2.04)	85% (x = 2.54)	90% (x = 2.69)
% Cation Exchange (ICP-OES)	71% (x = 2.13)	80% (x = 2.40)	82% (x = 2.46)
$[Cp_2Co]^+/[Et_4N]^+ = 1$[a]	24 h	48 h	72 h
% Cation Exchange (^{1}H NMR)[b]	56% (x = 1.69)	65% (x = 1.95)	68% (x = 2.04)
% Cation Exchange (ICP-OES)	53% (x = 1.59)	59% (x = 1.77)	60% (x = 1.80)

a) 0.02 M solution of $[Cp_2Co][PF_6]$ in acetone. b) Calculated based on the area of BTC, $[Cp_2Co]^+$ and $[Et_4N]^+$ respective peaks after digestion in DCl/d^6-dmso (1/5 v/v). See also Figures S14-S15.

Table S3. Iron and indium leaching in the reaction mixture during turnover of the catalyst $[(Fp\text{-}L)_{0.6}(TEA)_{2.4}][In_3(BTC)_4]$, measured by ICP-OES.

Days	In leaching	Fe leaching
1	0.02%	0.37%
2	0.00%	0.29%
3	0.02%	0.57%
4	0.01%	0.35%

Table S4. Percentage of TEA replaced by $[Fp\text{-}L]^+$ in $[(Fp\text{-}L)_{0.6}(TEA)_{2.4}][In_3(BTC)_4]$ before and after two catalytic cycles (96 h per cycle), measured by ICP-OES after digestion of the catalyst in HNO_3 (1/10 v/v).

Days	Before Diels-Alder	After Diels-Alder
8 (2 cycles)	21% (x = 0.63)	21% (x = 0.62)

Table S5. Crystallographic details.

Compound	**$[(Cp_2Co)_x(TEA)_{3-x}][In_3(BTC)_4]$**	**$[Cp_2Co]_3[In_3(BTC)_4]$**
Formula	$C_{12}H_4Co_{0.28}InO_8$	$C_{22}H_{14}CoInO_8$
M_r	407.57	580.08
CCDC number	1417098	1417097
Crystal System	cubic	Cubic
Space Group	$I\bar{4}3d$	$I\bar{4}3d$
a / Å	20.4031 (2)	20.4470 (1)
V / Å^3	8493.6 (3)	8548.48 (13)
Z	12	12
ρ_{calcd} / mg mm^{-3}	0.956[a]	1.352[a]
T [K]	100	100
Shape and color	Rod, Yellow	Block, Yellow
Size /mm	0.6 × 0.2 × 0.2	0.3 × 0.2 × 0.2
λ / Å	0.71073	0.71073
μ / mm^{-1}	1.01[a]	1.32[a]
Unique data	1686	2012
R_{int}	0.042	0.0428
Absorption correction	multi-scan	multi-scan
transmission max/min	1.000/0.824	1.0000/0.880
unique data [$F_o > 2\sigma F_o$)]	1585	1916
parameters/restraints	1686/51	129/180
Goof on F^2	1.243	1.188
R_1 [I>2σ (I)]	0.0627	0.0349
wR_2 [all data]	0.0651	0.0362
weighting scheme [w]	$1/[\sigma^2(F_o^2) + (0.1157P)^2 + 42.2172P]$[b]	$1/[\sigma^2(F_o^2) + (0.0867P)^2 + 2.6564P]$[b]
largest residuals [e Å^{-3}]	1.672, -0.599	0.602, -0.464

a) Solvent molecules are not included in the calculation since they are not detected in the single crystal structure. b) $P = 1/3[\max(F_o^2,0) + 2F_c^2]$

References

(1) Sheldrick, G. *Acta Crystallogr. Sect. A: Found. Crystallogr.* **2008**, *64*, 112.

(2) Allen, F. *Acta Crystallogr. Sect. B: Struct. Sci.* **2002**, *58*, 380.

(3) Le Bail, A. *Powder Diffr.* **2005**, *20*, 316.

(4) Genna, D. T.; Wong-Foy, A. G.; Matzger, A. J.; Sanford, M. S. *J. Am. Chem. Soc.* **2013**, *135*, 10586.

(5) Yu, J.; Cui, Y.; Wu, C.; Yang, Y.; Wang, Z.; O'Keeffe, M.; Chen, B.; Qian, G. *Angew. Chem., Int. Ed.* **2012**, *51*, 10542.

(6) Zheng, S.-T.; Bu, J. T.; Li, Y.; Wu, T.; Zuo, F.; Feng, P.; Bu, X. *J. Am. Chem. Soc.* **2010**, *132*, 17062.

(7) Chen, S.; Zhang, J.; Wu, T.; Feng, P.; Bu, X. *J. Am. Chem. Soc.* **2009**, *131*, 16027.